

Article

Characterization of the Erosion Basin Shaped by the Jet Flow of Sky-Jump Spillways

Raffaella Pellegrino  and Miguel Á. Toledo * 

Departamento de Ingeniería Civil, Hidráulica, Energía and Medio Ambiente, Universidad Politécnica de Madrid, 28040 Madrid, Spain

* Correspondence: miguelangel.toledo@upm.es

Abstract: The sky-jump spillway is an economical solution to return water to rivers, but an unsuitable flip bucket design might jeopardize the spillway, the dam, or other appurtenant works. Characterizing in advance, during the design phase, the position, size, and shape of the erosion basin would be useful to ensure that water flow is returned to the river in a safe way. Also, it would be useful for the safety assessment throughout the exploitation phase when erosion has not yet reached its maximum extension. Here, based on experimental laboratory work, the location, size, and shape of the erosion basin are analyzed, and a procedure is given for its characterization according to the design of the sky-jump spillway.

Keywords: hydraulic structure; sky-jump spillway; flip bucket; erosion basin; scour hole; jet flow

1. Introduction

The flip bucket is a structure that allows the evacuated water from the spillway of a dam to return to the riverbed. There are different types of buckets: horizontal, inclined, curved, with or without teeth [1]. A procedure for estimating the position, size, and shape of the erosion basin based on the sky jump geometric configuration is provided here. The depth of the erosion basin must be determined previously, something that has been extensively discussed by several authors. A good number of empirical formulas are available that allow us to establish, with a variable approximation, the depth of the erosion basin; on the other hand, the position, plant extension, and shape of the erosion basin have received little attention. Most of the formulas for estimating the scour depth are empirical and come from the calibration of relationships obtained by regression from experimental data obtained under different test conditions. The first investigation of the erosion depth downstream of a free-falling jet was developed by Schoklitsch [2], followed by Veronese [3], who developed an empirical formula that has served as a model for most later authors [4]. It has the limitation that the erosion depth was obtained for a quasi-vertical free fall jet. Yildiz and Üzücek [5] proposed a modified Veronese formula to take into account the incidence angle of the jet when impacting on the body of water. In addition to empirical formulas, physical models [6] or numerical methods [7–9] have been used. Neural network models have also been used [10,11] as an alternative to classical regression models. Some of the proposed formulas are simple and consider only two explanatory variables: the unit flow rate and the total head, as used by Veronese [3] and Damle et al. [12]; other formulas are more complex, such as those of Rubistein [13], Yuditsky [14], Mirskhulava [15], and Zvorykin [16], which contain parameters that are difficult to measure, such as the speed of the water flow before the impact, the thickness of the jet, the turbulence coefficient, and the depth of water flow at the lowest point of the sky jump. Doddiah et al. [17] consider time as an additional parameter. Another aspect that has been also taken into consideration over time is the effect of the emulsified air, as proposed by Ervine [18], Canepa and Hager [19], and later by Pagliara et al. [20]. Recent works evaluate scour by studying the dynamic



Citation: Pellegrino, R.; Toledo, M.Á. Characterization of the Erosion Basin Shaped by the Jet Flow of Sky-Jump Spillways. *Water* **2023**, *15*, 2930. <https://doi.org/10.3390/w15162930>

Academic Editor: Giuseppe Pezzinga

Received: 17 July 2023

Revised: 31 July 2023

Accepted: 8 August 2023

Published: 14 August 2023



Copyright: © 2023 by the authors. Licensee MDPI, Basel, Switzerland. This article is an open access article distributed under the terms and conditions of the Creative Commons Attribution (CC BY) license (<https://creativecommons.org/licenses/by/4.0/>).

pressures that are generated in the basin due to a free falling jet [21]. Other recent works assess the scour depth by studying the dynamic pressures that are generated in the basin taking into consideration the cushion due to the water mass [22].

Most of the formulas follow the general expression proposed by Mason [23]:

$$D = k \frac{q^x H^y}{d^z} \quad (1)$$

where, D is the total scour depth, measured from the surface of the tailwater depth (h_2); q is the unit flow; H is the difference in elevation between the reservoir level and the water surface downstream of the sky jump; and d the characteristic diameter of the particles. K, x, y, z are the constants to be determined. Some authors have considered additional variables, such as the flip angle (α) [5,24]. Few authors have tried to establish the size and position of the erosion basin by carrying out laboratory tests [25,26] or by applying neural networks [27]. Pagliara et al. [25,26] studied the characteristics of the erosion basin caused by a jet flowing out of pipes of different diameters and inclinations and proposed formulas for estimating the erosion depth, the position of the deepest point, and the width of the hole, which depend on the pipe diameter, the pipe inclination, the air content, the granulometry of the eroded material, and the fretwork downstream. They proposed an experimental equation for each of these variables. Azmathullah [10] applied nonlinear regression techniques to the data obtained from hydraulic models from other previous research works. He proposed formulas that allow the estimation of the total scour depth D . In addition, different techniques of computation were applied for the geometric characterization of the erosion basin, such as genetic expression programming and the adaptive neuro fuzzy inference system (ANFIS) [27]. A novel optimization algorithm HHO [28] was also proposed to improve the performance of an artificial neural network to predict scour depth; however, this study does not provide a formula for directly calculating the total scour depth.

A procedure is proposed in this paper to characterize the location, extent, and shape of the potential erosion basin as a function of the geometric parameters that define a cylindrical flip bucket. The total scour depth (D) can be determined using one of the available formulas (Table 1), most of which are also summarized by Castillo and Carrillo [29]. These formulas depend on the scour depth (t), the height of the water cushion (h_2), the total head (H), the unit flow (q), the grain diameter passing 50% or 90% of weight (d_{50}, d_{90}), the impingement jet angle (θ), the flip angle (α), and gravity (g). Using the total scour depth (D) widely studied by other authors, the main objective of this work is to fill a gap in the geometric characterization of the erosion basin downstream of a sky-jump spillway, providing formulas for determining the location, extent, and shape of the potential erosion basin depending of the flip bucket geometry. It should be noted that the estimation of the position, size, and shape of the erosion pit corresponds to a limit scour hole. In fact, the main goal of this study is not to predict a scour hole for a particular case but to provide a limit erosion case on the safety side regardless of soil heterogeneity and non-stationary mode of operation of the spillway. For this reason, we used an easily erodible sand, which is a material with low resistance. Furthermore, the limit scour hole is also independent of the non-stationary mode of operation of the spillway because the limit scour hole corresponds to a flow that has been maintained for a necessary time until erosion stops progressing.

Table 1. Empirical formulas that allow determining the basin potential erosion depth.

Authors		Erosion Depth (m)
Veronese B	[3]	$t + h_2 = 1.9 H^{0.225} q^{0.54}$
Damle A	[12]	$t + h_2 = 0.652 q^{0.5} H^{0.5}$
Damle B	[12]	$t + h_2 = 0.543 q^{0.5} H^{0.5}$
Damle C	[12]	$t + h_2 = 0.362 q^{0.5} H^{0.5}$

Table 1. *Cont.*

Authors		Erosion Depth (m)
INCYTH	[30]	$t + h_2 = 1.413q^{0.5}H^{0.25}$
Schoklitsch	[2]	$t + h_2 = 0.521 \frac{H^{0.2}q^{0.57}}{d_{90}^{0.52}}$
Veronese A	[3]	$t + h_2 = 0.202 \frac{q^{0.54}H^{0.225}}{d_{50}^{0.42}}$
Eggenberger	[31]	$t + h_2 = 1.44 \frac{q^{0.60}H^{0.50}}{d_{40}^{0.40}}$
Hartung	[32]	$t + h_2 = 1.40 \frac{q^{0.64}H^{0.36}}{d_{90}^{0.32}}$
Franke	[33]	$t + h_2 = 1.13 \frac{q^{0.67}H^{0.50}}{d_{50}^{0.50}}$
Mikhalev	[23]	$t + h_2 = \frac{1.804 q \sin \theta}{1 - 0.215 \cot \theta} \left(\frac{1}{d_{90}^{0.33} h_2^{0.5}} - \frac{1.126}{H} \right)$
Mirtskhulava	[15]	$t + h_2 = \left(\frac{0.97}{\sqrt{d_{90}}} - \frac{1.35}{\sqrt{H}} \right) \frac{q \sin \theta}{1 - 0.175 \cot \theta} + 0.25 h_2$
Chee and Kung	[24]	$t + h_2 = 3.30 H \left(\frac{q^2}{g H^3} \right)^{0.3} \left(\frac{H}{d} \right)^{0.1} \alpha^{0.1}$
Yildiz and Üzücek	[5]	$t + h_2 = 1.9H^{0.225}q^{0.54} \sin \theta$
Martins A	[34]	$t + h_2 = 0.14 N - 0.73 \frac{h_2^2}{N} + 1.7h_2$
Chian Min Wu	[23]	$t + h_2 = 1.18H^{0.235}q^{0.51}$
Martins B	[35]	$t + h_2 = 1.5 H^{0.1}q^{0.6}$
Taraimovich	[36]	$t + h_2 = 0.633H^{0.25}q^{0.67}$
Machado B	[37]	$t + h_2 = 2.98q^{0.5}H^{0.25}$
SOFRELEC	[38]	$t + h_2 = 2.3q^{0.6}H^{0.1}$
Kotoulas	[39]	$t + h_2 = 0.78 \frac{q^{0.7}H^{0.35}}{d_{30}^{0.4}}$
Chee and Padyar	[40]	$t + h_2 = 2.126 \frac{q^{0.67}H^{0.18}}{d_{50}^{0.063}}$
Bisaz and Tschopp	[41]	$t + h_2 = 2.76 q^{0.5}H^{0.25} - 7.22 d_{90}$
Chee and Kung	[24]	$t + h_2 = 1.663 \frac{q^{0.60}H^{0.20}}{d_{10}^{0.10}}$
Machado A	[37]	$t + h_2 = 1.35 \frac{q^{0.5}H^{0.3145}}{d_{90}^{0.0645}}$
Jaeger	[42]	$t + h_2 = 0.6 H^{0.25}q^{0.5} \left(\frac{h_2}{d_{50}} \right)^{0.333}$
Rubinstein	[13]	$t + h_2 = h_2 + 2.59h_2 \left(\frac{H+h_2}{d_{90}} \right)^{0.75} \frac{q^{1.20}}{13.70 H^{1.80}} \left(\frac{H}{h_2} \right)^{1.33}$
Mason and Arumugam	[43]	$t + h_2 = 3.27 \frac{q^{0.60}H^{0.05}h_2^{0.15}}{d_{30}^{0.30}d_{50}^{0.10}}$
Ghodsian et al.	[44]	$t + h_2 = 0.75h_2 \left(\frac{q}{(h_2^3g)^{0.5}} \right)^{0.524} \left(\frac{d_{50}}{h_2} \right)^{-0.366} \left(\frac{H}{h_2} \right)^{0.255}$ $N = 0.007 \sqrt[7]{\frac{Q^3 H^{1.5}}{d_{90}^2}}$

2. Materials and Methods

2.1. General Approach

This research was developed in four phases (Figure 1). The first phase is analysis, allowed to identify the relevant parameters for the objective pursued. In the second phase, physical modeling was developed in four steps. Initially, the experimental test campaign was defined. This was followed by the design and construction of the test facility, with all the necessary instrumentation. After that, the test protocol was defined to finally perform the tests foreseen in the programming step. From the obtained data through physical modeling, the third phase consisted of the calibration and subsequent validation of the empirical formulas that allow characterizing the erosion hole based on the geometric characteristics of the flip bucket. Finally, in the fourth and final phase, a procedure was defined and validated to characterize the erosion hole based on the geometric characteristics of the flip bucket of the spillway.

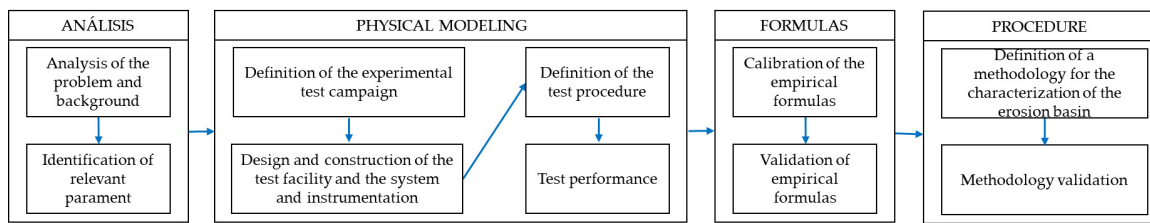


Figure 1. Research phases.

2.2. Relevant Parameters

The unit flow (q) and the difference between the water level at the reservoir and the water level downstream of the dam (H) are the parameters that most influence the depth of scour [45]. As previously commented, there are formulas that, in addition to the parameters q and H , consider the tailwater depth (h_2), or the equivalent diameter of the eroded material (d). To study how the geometry of the flip bucket can affect the formation of the erosion basin, in addition to q , H and h_2 , two other parameters are defined: the radius (R) and the flip angle (α) of the flip bucket. The radius of a flip bucket is usually defined in relation to the h_b , the water height at the launching point: $R \geq 4 h_b$ or $R \geq 5 h_b$, respectively, according to Peterka [46] and USBR [4]. The flip bucket usually varies between 15° and 40° [46–48]. Although there are numerous exceptions, it is unusual for the flip angle to exceed 45° . The flip angle, together with the jet speed, influences the distance where the impact occurs in the river bed or in the erosion basin. Anyway, this distance also depends, in addition to total height (H) and the tailwater depth (h_2), on the height of the lip of the flip bucket over the ground (z_p). Finally, the considered parameters are flow discharge (Q), total height (H), distance between the lip of the flip bucket and the level at the reservoir (z_0), flip bucket radius (R), launching angle (α), height of the flip bucket lip over the ground (z_p), height of the lip of the flip bucket over the tailwater (z_1), tailwater depth (h_2), scour depth (t), total scour depth (D), distance of maximum scour from the bucket lip (L_c) (Figure 2), semi-axis length (A_1) in the direction of flow from the maximum scour point to the furthest downstream point, semi-axis length (A_2) in the direction of flow from the maximum scour point towards the furthest point upstream, total length (A) in the river longitudinal direction, semi-axis length (B_1) in the transverse direction to the flow from the maximum scour point towards the furthest point towards the hydraulic right (whose semi-axis length B_2 in the transverse direction to the flow from the maximum scour point to the furthest point to the hydraulic left), total width B , and shape parameter A/B , which we will call the circularity index (Figure 3).

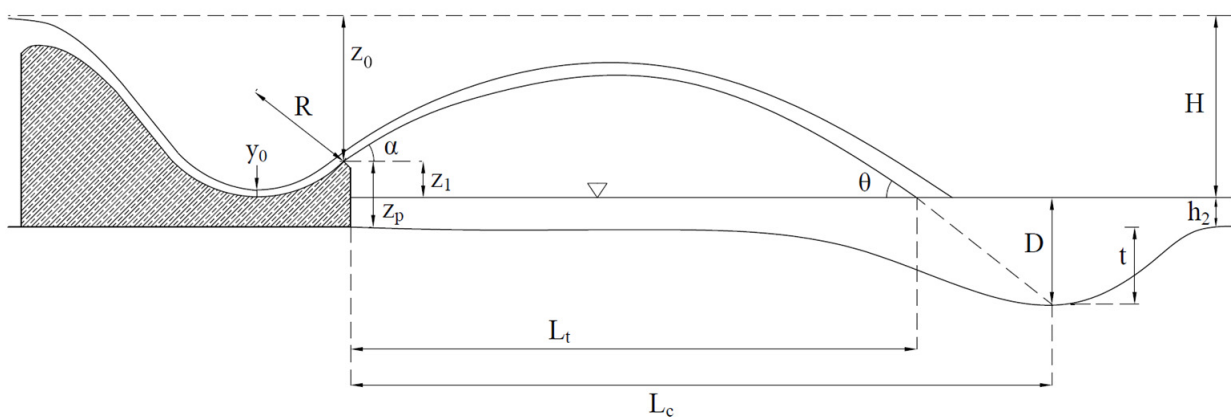


Figure 2. Longitudinal profile with involved parameters.

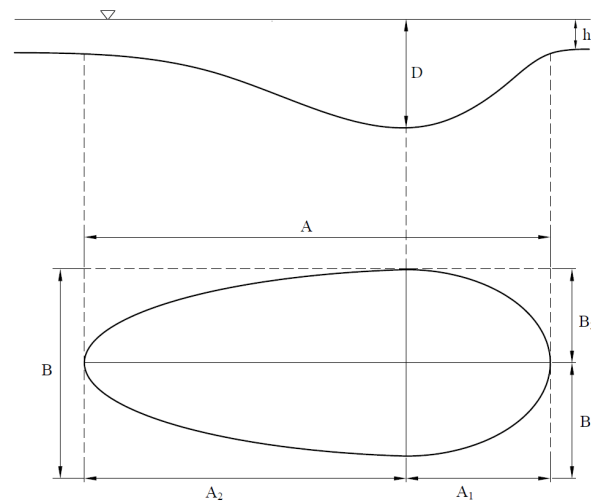


Figure 3. Longitudinal profile and plan of the erosion.

2.3. Physical Modeling

2.3.1. Experimental Set-Up

The tests were carried out in a channel 2.46 m wide, 1.30 m high and 13.7 m long. It is divided into three functional zones (Figure 4). The first zone is for water supply and energy dissipation. The second one is the testing area, with a length of 6.37 m, which is filled with sand up to a height of 0.50 m and is limited upstream by a wall. The sky-jump spillway is positioned in the middle of that wall. On the left side of the channel, in the direction of the flow, there is a 4.60 m long and 1.1 m high glass window, which enables visual inspection, video filming and side photography. In the third and final zone of the testing channel, there is a decanting pond to prevent any dragged material from reaching the tank, which is under the laboratory floor. Given the height limitation of the test channel and the need to have a sand thickness of 0.50 m, a height of 0.60 m was set for the spillway piece. The spillway sides are made of methacrylate (Figure 5) in order to make visible the flow of water on the sky jump. For the tests with the 0.06 m water cushion, a wooden bar sealed with silicone is positioned on top of the wall downstream of the testing area (Figure 5). For more detail on the physical model, the work of Pellegrino et al. [49] can be consulted.

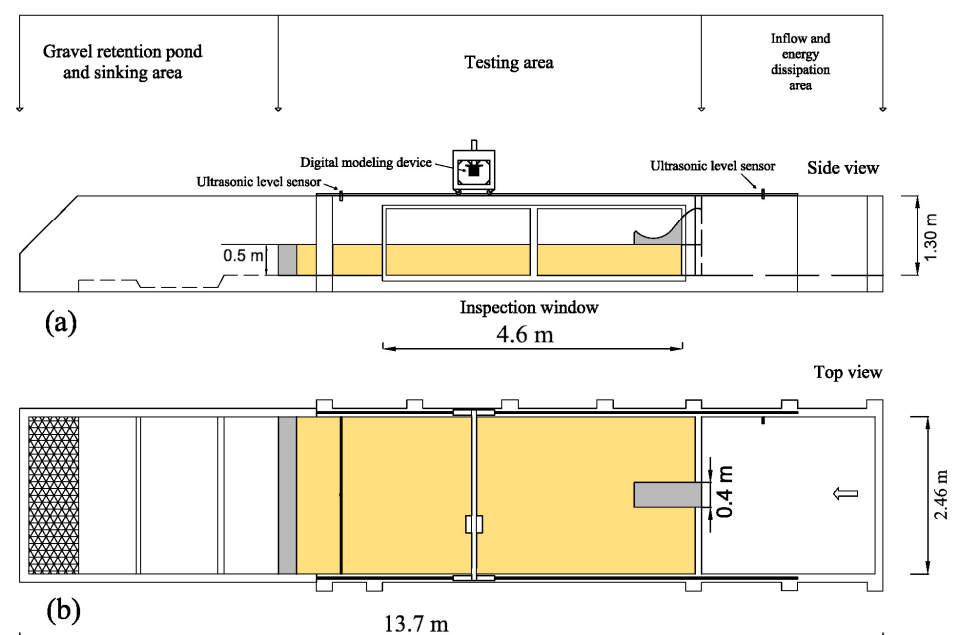


Figure 4. Testing set-up: (a) side view; (b) plan view.



Figure 5. (a) Testing area with spillway. Case: $R = 0.4$ m; $\alpha = 45^\circ$; (b) view of the testing channel from downstream with a water cushion.

The facility has a 2D-laser scanner (SICK LMS200-30106, SICK AG Waldkirch, Germany) that was used to obtain the digital terrain model (DTM) before and after erosion occurred. The laser scanner is mounted on a motorized mobile structure controlled by a computer using an algorithm developed in LabView. The data obtained from the scanner are stored directly in a .txt file, and then, the DTM is obtained using the Arc-Gis tool.

As the objective of this work is to estimate the position, dimensions, and shape of the scour hole independently of the material that makes up the bed, the size of the material remained constant and small enough. Veronese [3] already observed that for a material with a size smaller than 5 mm, the erosion depth is independent of the particle size; it was later confirmed by Machado [37] and Breusers [50]. We used an easily erodible sand with a d_{50} of 0.6 mm.

2.3.2. Test Procedure

Once the sky-jump spillway is positioned, the material is leveled and the surface of the moving bed is scanned before testing as a reference for the subsequent determination of the volume of eroded material. In the case of the tests with a water cushion 0.06 m deep, the filling with water is carried out slowly, approximately in five hours, to avoid material dragging. To verify that there was no significant settlement due to the drainage of water before scanning the erosion hole, two scans of the leveled ground were carried out, one before filling with water and another one after the slow drainage of interstitial water. From the comparison of those two DTMs, it was observed that the mean settlement was less than 1 cm. That magnitude is similar to that of the scan interval, 1 cm, that was set for scanning with the laser. Also, it is similar to the cell size used to generate the MDTs, 1 cm again. So, it can be assumed that the settlements due to the loss of interstitial water are not relevant and, consequently, that the only significant settlements are caused by the erosion process. Given the rapid erosion speed, the duration of each test was set at 12 min from the start of the spilling. The testing flow rates were obtained by opening the motorized valve for 17 s, 18 s, and 20 s, which corresponds to flow rates of 37.5 L/s, 42 L/s and 50 L/s, respectively. After each test, we waited 24 h to completely drain the canal, including the interstitial water, before scanning the surface of the eroded sandy bed (Figure 6).

The transversal profiles were obtained by means of the laser scanner every centimeter along the 2.46 m of total width. Data were stored in a text format file where the x , and z coordinates are specified for each point. Using this file and the Arc-Gis 10.3.1 software, the digital terrain model (DTM) of the scour hole was obtained for every test. To determine the maximum scour depth (t), the heights of the DTM obtained before and after the erosion were subtracted at every point of the mesh.

3. Results and Discussion

In the present work, experimental formulas are provided that characterize the erosion hole: position of the maximum erosion point (L_c), maximum length (A), maximum width (B), and circularity index (A/B). For the estimation of maximum depth, many formulas are available from different authors. As the erosion process is a complex physical phenomenon and it depends on the nature of the bed, rock, or soil, this work introduces the concept of limit erosion basin, and in fact the results are here summarized and analyzed for each parameter defining the limit scour hole position, size, and shape.

The limit scour hole is a pit that is formed in a fine-grained soil that may not be achieved in each real case. In fact, if the bed is made of rock, the resistance to erosion is greater than in a soil bed, so it can be affirmed that using sand corresponds to making an estimation on the safety side.

With the awareness that the risk of destruction of a structure due to a specific cause is generally difficult to determine, the procedure proposed in this work to estimate the position and size of the limit erosion basin provides a tool to assess in advance whether the erosion basin can affect adjacent structures or the spillway or dam itself. If results obtained by applying the proposed procedure indicate that the erosion does not affect the mentioned structures, it can be deduced that there will be no affectation. On the other hand, if it affects the mentioned structures, there is no certainty that the condition will occur, and more detailed studies would be required to obtain robust conclusions because in this case it would also be necessary to consider the dimensions of the limit erosion basin depending on the flows evacuated, their duration, and the quality of bed material where the spillway jet impacts. In addition, this procedure can be useful for the design of a pre-excavated scour hole.

In the present work, experimental formulas are provided that characterize the limit erosion hole: position of the maximum erosion point (L_c), maximum length (A), maximum width (B), and circularity index (A/B). For the estimation of maximum depth, many formulas are available from different authors. The results are here summarized and analyzed for each parameter defining the scour hole position, size, and shape.

The multiple linear regression techniques were applied to estimate the geometric characteristics of the limit erosion hole. The target variables are: the position of the maximum erosion point (L_c), the maximum length (A), defined as the sum of two semi-axes (A_1) and (A_2), and the circularity index (A/B). The explanatory variables are: the radius of the flip bucket (R), the impingement angle (θ), the scour depth (t), and the difference in height (z_1) between the lip of the flip bucket and the downstream water level (h_2).

The experimental formulas were firstly calibrated and then validated; 60% of the 54 tests performed were used to calibrate the formulas. Subsequently, the relationships obtained were validated using the remaining 40% of the tests. The validation tests were chosen randomly but ensuring that all geometric typologies were included and that, for each one of them, the two conditions were also included, with and without initial cushion of water downstream. The coefficient of determination (R^2), absolute mean error (MAE), and relative mean error (MRE) were determined for every formula.

3.1. Erosion Depth

3.1.1. Estimation of Erosion Depth

If the experimental data of total scour depth (D_{exp}) are compared with data calculated with the formulas detailed in the introduction of this article, it is observed that the formulas that best approximate the experimental data vary according to the calculation of H .

During the laboratory test, the value of parameter H varies depending on the water level downstream (h_2). The initial condition is the one that is established before starting the test, and the parameter h_2 can assume only two values, 0.00 m and 0.06 m, while the stationary condition is the one that corresponds to the instant in which the entire test channel contributes to the drainage of the flow from the spillway; in this case, the value of h_2 will depend on this flow. It is indicated with h_2 the height of the water depth cushion

in the initial condition. Then, with h_{2s} , the height of the water cushion is the stationary condition. For each experimental test, two values of experimental total scour depth (D_{exp}) are obtained, one relating on the initial condition and the other relating to the stationary condition. Total scour depth can also be calculated by applying the literature formulas in the two conditions indicated above. For each condition, the experimental (D_{exp}) and calculated (D_{cal}) value of total scour depth are compared using the mean absolute error (MAE) and the mean relative error (MRE) (Figure 7). In the tests without a water cushion, it was observed that the erosion developed before a height cushion h_{2s} (stationary condition) was established, different from the initial value h_2 (initial condition). For the calculation of the MAE and MRE between the experimental and calculated data of total scour (D), two conditions were considered: the initial condition where h_2 can assume values equal to 0.00 m or 0.06 m and the stationary condition where the value of h_{2s} also depends on the flow drained by the spillway (Table 3).

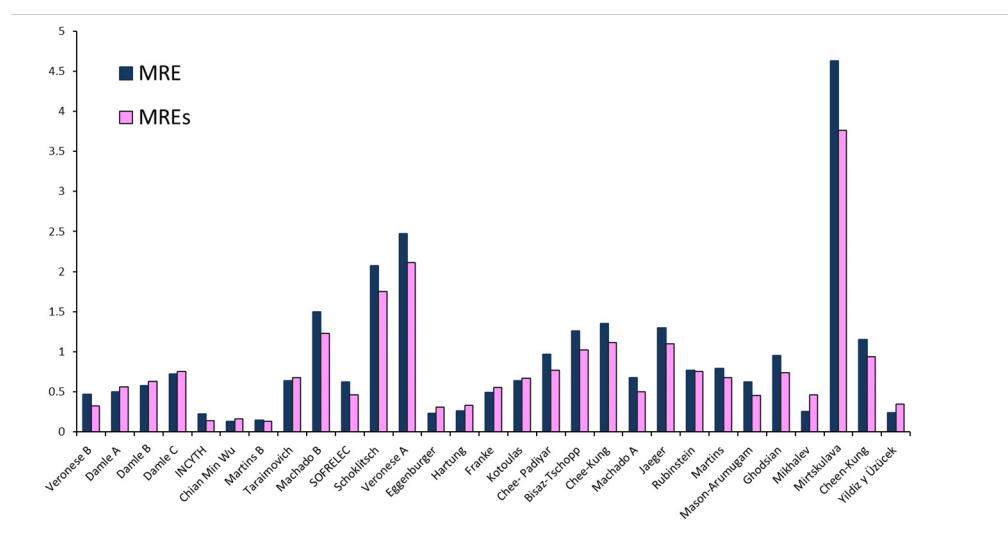


Figure 7. Comparing the experimental and calculated data of the total scour (D) with mean relative error in the initial condition (MRE) and in the stationary condition (MREs).

Table 3. Mean absolute error and mean relative error for the initial condition (MAE and MRE) and stationary condition (MAEs and MREs) obtained by comparing the experimental and calculated data of the total scour (D).

Author		MAE (m)	MRE	MAEs (m)	MREs
Veronese B	[3]	0.159	0.47	0.116	0.32
Damle A	[12]	0.188	0.50	0.230	0.56
Damle B	[12]	0.218	0.58	0.259	0.63
Damle C	[12]	0.268	0.72	0.308	0.75
INCYTH	[30]	0.072	0.22	0.054	0.14
Chian Min Wu	[23]	0.050	0.13	0.069	0.16
Martins B	[35]	0.053	0.15	0.055	0.13
Taraimovich	[36]	0.238	0.64	0.277	0.68
Machado B	[37]	0.528	1.50	0.479	1.23
SOFRELEC	[38]	0.214	0.62	0.174	0.46
Schoklitsch	[2]	0.734	2.07	0.686	1.75
Veronese A	[3]	0.878	2.47	0.827	2.11
Eggenberger	[31]	0.090	0.23	0.132	0.31
Hartung	[32]	0.100	0.26	0.141	0.33
Franke	[33]	0.184	0.49	0.225	0.55
Kotoulas	[39]	0.237	0.64	0.275	0.67
Chee-Padiyar	[40]	0.340	0.97	0.297	0.77

Table 3. *Cont.*

Author		MAE (m)	MRE	MAEs (m)	MREs
Bisaz-Tschopp	[41]	0.443	1.26	0.396	1.02
Chee-Kung	[24]	0.477	1.350	0.432	1.11
Machado A	[37]	0.234	0.68	0.188	0.50
Jaeger	[42]	0.461	1.299	0.430	1.099
Rubinstein	[13]	0.283	0.765	0.313	0.756
Martins A	[34]	0.293	0.791	0.282	0.680
Mason-Arumugam	[43]	0.216	0.620	0.176	0.451
Ghodsian	[44]	0.336	0.952	0.296	0.739
Mikhalev	[23]	0.087	0.253	0.185	0.464
Mirtskulava	[15]	1.687	4.628	1.493	3.758
Cheen-Kung	[24]	0.418	1.151	0.369	0.937
Yildiz and Üzücek	[5]	0.083	0.237	0.145	0.349

It can be observed that the formulas that best fit the experimental data are those of INCYTH [30], Chian Min Wu [23], Martins B [35], Eggenberger [31], Hartung [32], Mikhalev [23], and Yildiz and Üzücek [5] in the initial condition, while in the stationary condition the formulas of INCYTH [30], Chian Min Wu [23] and Martins B [35] have a better adjustment.

In practice, the initial condition corresponds to a poorly resistant bed; on the contrary, the stationary condition, influenced by the evacuated flow, corresponds to a resistant bed. Therefore, it is necessary to consider the type of bed to determine the scour depth. The initial condition is considered in the present study, taking into account that the sandy bed has a very low resistance to erosion.

3.1.2. Influence of the Flip Bucket Radius

The results of the tests show a moderate but clear influence of radius on the depth of erosion (Figure 8). It is observed that for the same flip angle (α), the depth of erosion (t) increases when the radius (R) is reduced. Moreover, the effect of the radius is greater for greater angles. To quantify the influence of radius on scour, the flip angle (α), flow rate (Q), and height of the tailwater (h_2) were fixed, and the absolute error (AE) and relative error (RE) were calculated taking the depth (t), marked in blue, corresponding to the greater radius ($R = 0.4$ m) as a reference (Table 4). In the case of a flip angle of 30° , where there is a lack of experimental data, the relative error (RE) has been calculated taking the depth (t) corresponding to the radius equal to 0.30 m; to distinguish this situation, the results have been highlighted in yellow.

Table 4. Absolute errors (AR) and relative errors (RE) of the scour depth (t) with respect to the greater radius ($R = 0.4$ m) marked in blue for different value of flip angle (α). The relative error, highlighted in yellow, has been calculated taking the depth (t) corresponding to the radius equal to 0.30 m.

(a) ($h_2 = 0.0$ m)						
Practice	Q (l/s)	α (°)	R (m)	t (m)	AR (m)	RE
A2_h0_17	37.5	15	0.2	0.321	0.062	0.24
B2_h0_17	37.5	15	0.3	0.291	0.032	0.12
C2_h0_17	37.5	15	0.4	0.259	-	-
A2_h0_18	42.0	15	0.2	0.332	0.061	0.23
B2_h0_18	42.0	15	0.3	0.310	0.039	0.14
C2_h0_18	42.0	15	0.4	0.271	-	-
A2_h0_20	50.0	15	0.2	0.34	0.055	0.19
B2_h0_20	50.0	15	0.3	0.329	0.044	0.16
C2_h0_20	50.0	15	0.4	0.285	-	-

Table 4. Cont.

(b) ($h_2 = 0.0$ m)						
Practice	Q (l/s)	α (°)	R (m)	t (m)	AR (m)	RE
A3_h0_17	37.5	30	0.2	0.416	0.049	0.13
B3_h0_17	37.5	30	0.3	0.367	-	-
C3_h0_17	37.5	30	0.4	-	-	-
A3_h0_18	42.0	30	0.2	0.436	0.048	0.12
B3_h0_18	42.0	30	0.3	0.388	-	-
C3_h0_18	42.0	30	0.4	-	-	-
A3_h0_20	50.0	30	0.2	0.441	0.034	0.08
B3_h0_20	50.0	30	0.3	0.407	-	-
C3_h0_20	50.0	30	0.4	-	-	-
(c) ($h_2 = 0.0$ m)						
Practice	Q (l/s)	α (°)	R (m)	t (m)	AR (m)	RE
A4_h0_17	37.5	45	0.2	0.457	0.108	0.31
B4_h0_17	37.5	45	0.3	0.405	0.056	0.16
C4_h0_17	37.5	45	0.4	0.349	-	-
A4_h0_18	42.0	45	0.2	0.475	0.114	0.32
B4_h0_18	42.0	45	0.3	0.421	0.060	0.17
C4_h0_18	42.0	45	0.4	0.361	-	-
A4_h0_20	50.0	45	0.2	0.490	0.087	0.22
B4_h0_20	50.0	45	0.3	0.443	0.040	0.10
C4_h0_20	50.0	45	0.4	0.403	-	-
(d) ($h_2 = 0.06$ m)						
Practice	Q (l/s)	α (°)	R (m)	t (m)	AR (m)	RE
A2_h6_17	37.5	15	0.2	0.264	0.029	0.12
B2_h6_17	37.5	15	0.3	0.253	0.018	0.08
C2_h6_17	37.5	15	0.4	0.235	-	-
A2_h6_18	42.0	15	0.2	0.285	0.035	0.14
B2_h6_18	42.0	15	0.3	0.275	0.025	0.10
C2_h6_18	42.0	15	0.4	0.250	-	-
A2_h6_20	50.0	15	0.2	0.303	0.034	0.13
B2_h6_20	50.0	15	0.3	0.291	0.022	0.08
C2_h6_20	50.0	15	0.4	0.269	-	-
(e) ($h_2 = 0.06$ m)						
Practice	Q (l/s)	α (°)	R (m)	t (m)	AR (m)	RE
A3_h6_17	37.5	30	0.2	0.317	0.042	0.15
B3_h6_17	37.5	30	0.3	0.275	-	-
C3_h6_17	37.5	30	0.4	-	-	-
A3_h6_18	42.0	30	0.2	0.320	0.021	0.07
B3_h6_18	42.0	30	0.3	0.299	-	-
C3_h6_18	42.0	30	0.4	-	-	-
A3_h6_20	50.0	30	0.2	0.328	0.01	0.03
B3_h6_20	50.0	30	0.3	0.318	-	-
C3_h6_20	50.0	30	0.4	-	-	-

Table 4. Cont.

(f) ($h_2 = 0.06$ m)						
Practice	Q (l/s)	α (°)	R (m)	t (m)	AR (m)	RE
A4_h6_17	37.5	45	0.2	0.385	0.101	0.36
B4_h6_17	37.5	45	0.3	0.367	0.083	0.29
C4_h6_17	37.5	45	0.4	0.284	-	-
A4_h6_18	42.0	45	0.2	0.410	0.113	0.38
B4_h6_18	42.0	45	0.3	0.380	0.083	0.28
C4_h6_18	42.0	45	0.4	0.297	-	-
A4_h6_20	50.0	45	0.2	0.440	0.122	0.38
B4_h6_20	50.0	45	0.3	0.423	0.105	0.33
C4_h6_20	50.0	45	0.4	0.318	-	-

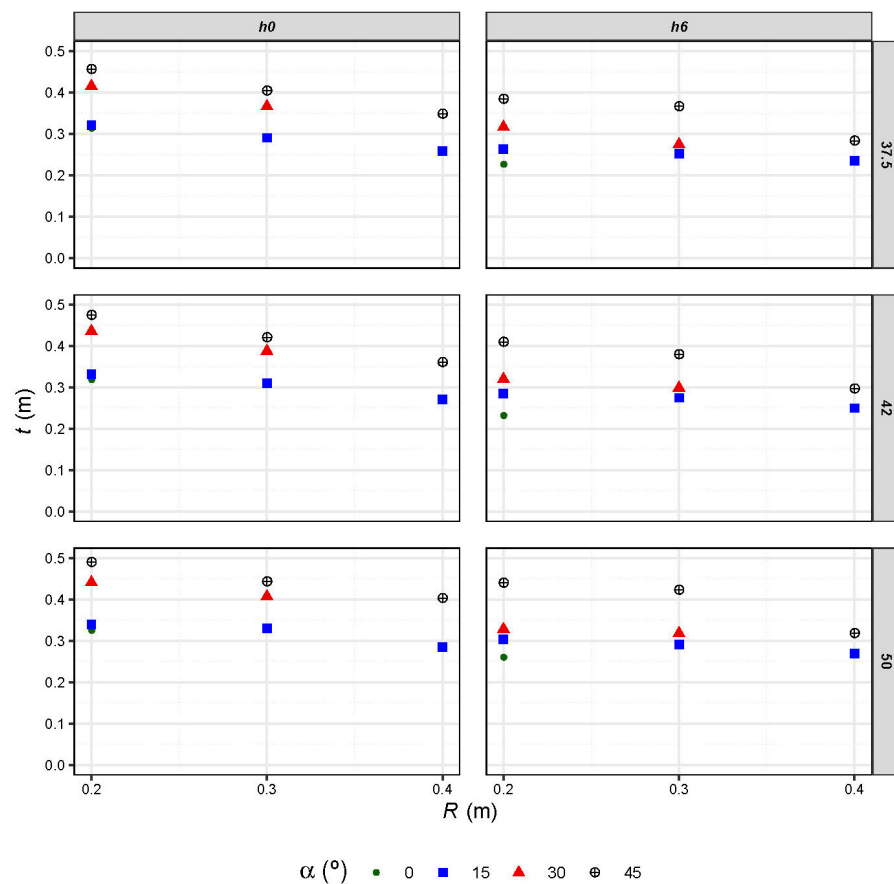


Figure 8. Evolution of scour depth (t) with the radius (R), separating the data, for each flip angle (α), by height of the water cushion (h_0 , without cushion, and h_6 , with cushion of 0.06 m) and by test flow rate (37.5 L/s, 42 L/s and 50 L/s).

The scour depth increases 25% on average when the radius decrease from 0.40 m to 0.20 m. This difference is significant and might be a reason to design the flip bucket with a radius greater than the minimum necessary, although this increases the flip bucket cost.

3.1.3. Influence of the Flip Angle

The results of the tests clearly show that erosion increases as the flip angle (α) becomes greater (Figure 9).

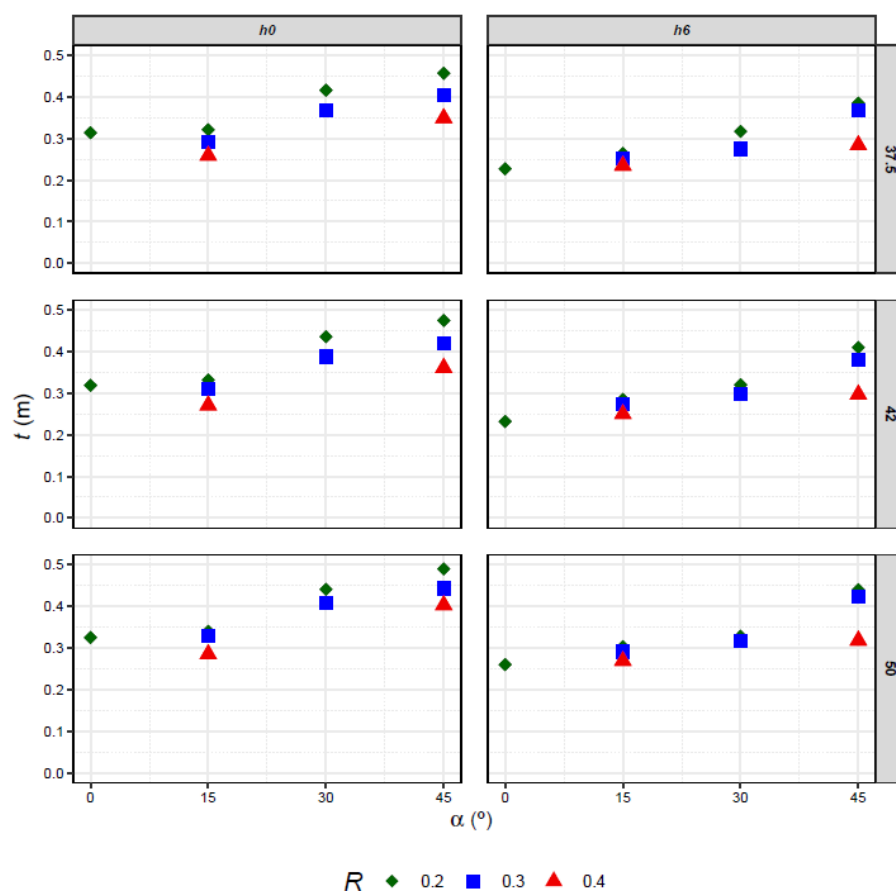


Figure 9. Evolution of scour depth (t) with the flip angle (α), separating the data, for each radius, by height of the water cushion (h_0 , without cushion, and h_6 , with cushion of 0.06 m) and by test flow rate (37.5 L/s, 42 L/s and 50 L/s).

To quantify the influence of the flip angle on the scour depth (t), the radius (R), the flow rate (Q), and the water cushion (h_2) were fixed, and the absolute error (AE) and the relative error (RE) were calculated taking the scour depth (t) marked in blue corresponding to the greater angle ($\alpha = 45^\circ$) as a reference (Table 5).

Table 5. Absolute errors (AR) and relative errors (RE) of the scour depth (t) with respect to the greater flip angle ($\alpha = 45^\circ$) marked in blue, for different values of radius (R).

(g) ($h_2 = 0.00$ m)						
Practice	Q (l/s)	α (°)	R (m)	t (m)	AR (m)	RE
A2_h0_17	37.5	15	0.2	0.321	0.136	0.30
B2_h0_17	37.5	30	0.2	0.416	0.041	0.09
C2_h0_17	37.5	45	0.2	0.457	-	-
A2_h0_18	42.0	15	0.2	0.332	0.143	0.30
B2_h0_18	42.0	30	0.2	0.436	0.039	0.08
C2_h0_18	42.0	45	0.2	0.475	-	-
A2_h0_20	50.0	15	0.2	0.340	0.150	0.31
B2_h0_20	50.0	30	0.2	0.441	0.049	0.10
C2_h0_20	50.0	45	0.2	0.490	-	-

Table 5. Cont.

(h) ($h_2 = 0.0$ m)						
Practice	Q (l/s)	α (°)	R (m)	t (m)	AR (m)	RE
A3_h0_17	37.5	15	0.3	0.291	0.114	0.28
B3_h0_17	37.5	30	0.3	0.367	0.038	0.09
C3_h0_17	37.5	45	0.3	0.405	-	-
A3_h0_18	42.0	15	0.3	0.310	0.111	0.26
B3_h0_18	42.0	30	0.3	0.388	0.033	0.08
C3_h0_18	42.0	45	0.3	0.421	-	-
A3_h0_20	50.0	15	0.3	0.330	0.113	0.26
B3_h0_20	50.0	30	0.3	0.407	0.036	0.08
C3_h0_20	50.0	45	0.3	0.443	-	-
(i) ($h_2 = 0.0$ m)						
Practice	Q (l/s)	α (°)	R (m)	t (m)	AR (m)	RE
A4_h0_17	37.5	15	0.4	0.259	0.09	0.26
B4_h0_17	37.5	30	0.4	-	-	-
C4_h0_17	37.5	45	0.4	0.349	-	-
A4_h0_18	42.0	15	0.4	0.271	0.09	0.25
B4_h0_18	42.0	30	0.4	-	-	-
C4_h0_18	42.0	45	0.4	0.361	-	-
A4_h0_20	50.0	15	0.4	0.285	0.118	0.29
B4_h0_20	50.0	30	0.4	-	-	-
C4_h0_20	50.0	45	0.4	0.403	-	-
(j) ($h_2 = 0.06$ m)						
Practice	Q (l/s)	α (°)	R (m)	t (m)	AR (m)	RE
A2_h6_17	37.5	15	0.2	0.264	0.121	0.31
B2_h6_17	37.5	30	0.2	0.317	0.068	0.18
C2_h6_17	37.5	45	0.2	0.385	-	-
A2_h6_18	42.0	15	0.2	0.285	0.125	0.30
B2_h6_18	42.0	30	0.2	0.320	0.09	0.22
C2_h6_18	42.0	45	0.2	0.410	-	-
A2_h6_20	50.0	15	0.2	0.303	0.137	0.31
B2_h6_20	50.0	30	0.2	0.328	0.112	0.25
C2_h6_20	50.0	45	0.2	0.440	-	-
(k) ($h_2 = 0.06$ m)						
Practice	Q (l/s)	α (°)	R (m)	t (m)	AR (m)	RE
A3_h6_17	37.5	15	0.3	0.253	0.114	0.31
B3_h6_17	37.5	30	0.3	0.275	0.092	0.25
C3_h6_17	37.5	45	0.3	0.367	-	-
A3_h6_18	42.0	15	0.3	0.275	0.105	0.28
B3_h6_18	42.0	30	0.3	0.299	0.081	0.21
C3_h6_18	42.0	45	0.3	0.380	-	-
A3_h6_20	50.0	15	0.3	0.291	0.132	0.31
B3_h6_20	50.0	30	0.3	0.318	0.105	0.25
C3_h6_20	50.0	45	0.3	0.423	-	-

Table 5. Cont.

(l) ($h_2 = 0.06$ m)						
Practice	Q (l/s)	α (°)	R (m)	t (m)	AR (m)	RE
A4_h6_17	37.5	15	0.4	0.235	0.049	0.17
B4_h6_17	37.5	30	0.4	-	-	-
C4_h6_17	37.5	45	0.4	0.284	-	-
A4_h6_18	42.0	15	0.4	0.250	0.047	0.16
B4_h6_18	42.0	30	0.4	-	-	-
C4_h6_18	42.0	45	0.4	0.297	-	-
A4_h6_20	50.0	15	0.4	0.269	0.049	0.15
B4_h6_20	50.0	30	0.4	-	-	-
C4_h6_20	50.0	45	0.4	0.318	-	-

Scour depth (t) increases 27% on average when angle changes from 15° to 45°. This difference is significant and might be a reason to design the flip bucket with a smaller flip angle. Furthermore, the effect of the flip angle increases when the radius is the lower value, 0.20 m.

3.2. Position of the Point of Maximum Erosion Depth

The parameter L_c defines the distance in plan from the lip of the flip bucket to the point where erosion depth is maximum. It is observed that L_c increases for values of α between 0° and 30°; however, it decreases for 45° (Figure 10). We should take into consideration that there are two opposite effects: (a) when the angle increases, up to 45°, the impact on the terrain surface occurs farther away from the flip bucket; (b) also, when the angle increases, the jet impacts the ground with a more vertical direction, which implies that erosion moves less downstream and develops more in the vertical direction, causing a deeper erosion. As a consequence, an increase in the flip angle might result in a greater or lower L_c , depending on the prevalence of one of the two mentioned effects

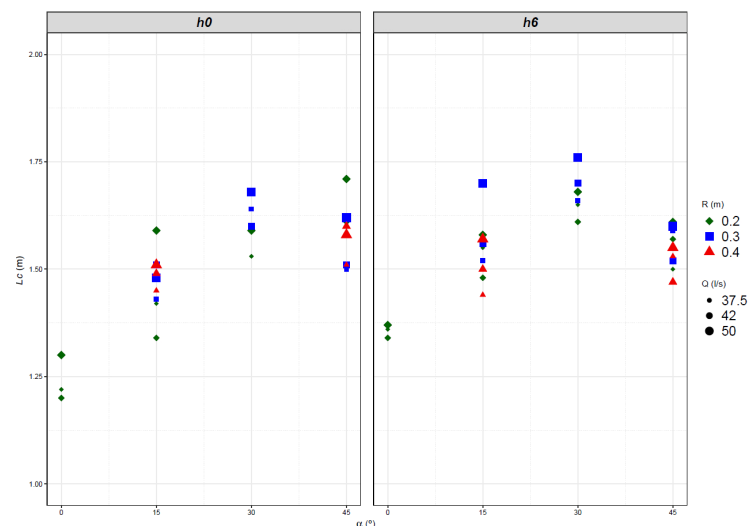


Figure 10. Evolution of the position of the point of maximum erosion depth L_c with the flip angle (α), separating the cases without cushion h_0 and with cushion h_6 and distinguishing by size the different flows (37.5, 42.0, 50.0 L/s) and by shape and color the radii (0.2, 0.3 and 0.4 m).

For the calculation of the position of the point with maximum erosion depth L_c , two linear regressions were performed: one considering the parameter t/z_1 and the impingement angle (θ) and another considering t/z_1 and the radius (R). Calibration and validation sets were separated. The first formula (Equation (2)) presents an R^2 of 0.982, and MAE_v equal to 0.19 m and an MRE_v of 12.76%, corresponding to the validation set. The second formula

(Equation (3)) presents an R^2 of 0.971, an MAEv equal to 0.265 m, and an MREv of 17.44%. Although the first equation is more precise, R is directly available data, while θ must be determined [51].

$$\frac{L_c}{z_1} = \left(5.76 \frac{t}{z_1} - 0.1 \theta \right) \tag{2}$$

$$\frac{L_c}{z_1} = \left(5.28 \frac{t}{z_1} - 3.97 R \right) \tag{3}$$

Equations (2) and (3) express linear relations between L_c/z_1 and θ and R , respectively. This function was represented together with the experimental data. (Figures 11 and 12). We can observe a reasonable correspondence with the experimental values, as expected from the error quantification. Furthermore, the parameter L_c/z_1 decreases when the impingement angle (θ) increases. As expected, the existence of a water cushion clearly affects the position of the point with maximum erosion depth. When there is a water cushion, the geometry of the flip bucket has a more significant influence on the parameter L_c/z_1 (Figure 13).

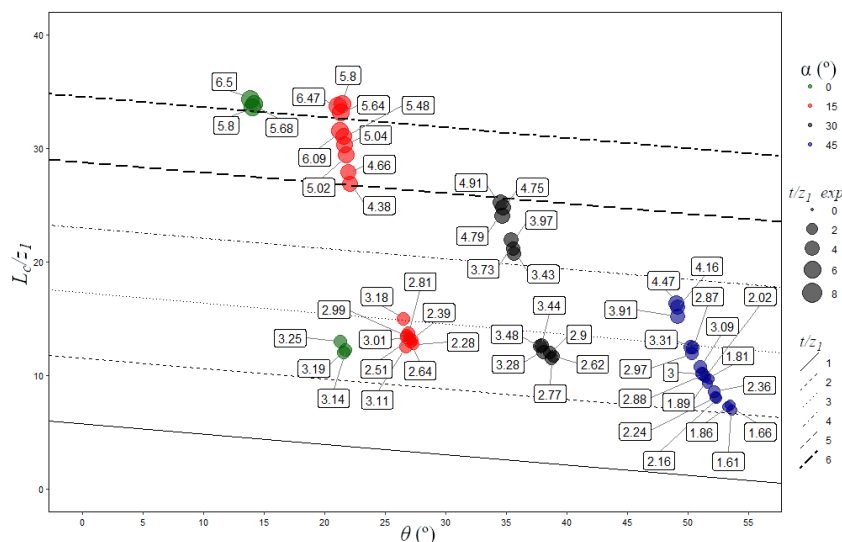


Figure 11. Results obtained for L_c/z_1 with the Equation (2) for several values of t/z_1 and impingement angle (θ). The experimental value of t/z_1 is indicated next to each point.

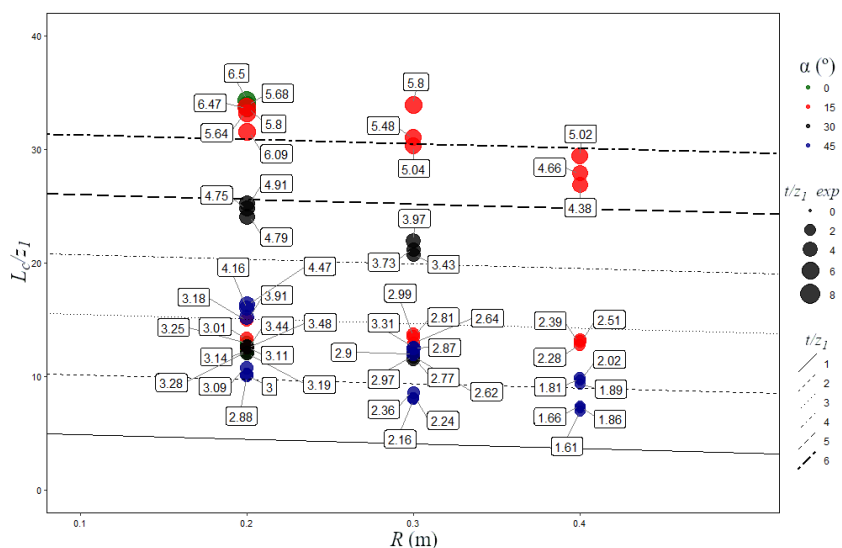


Figure 12. Results obtained for L_c/z_1 with the Equation (3) for several values of t/z_1 and radius (R). The experimental value of t/z_1 is indicated next to each point.

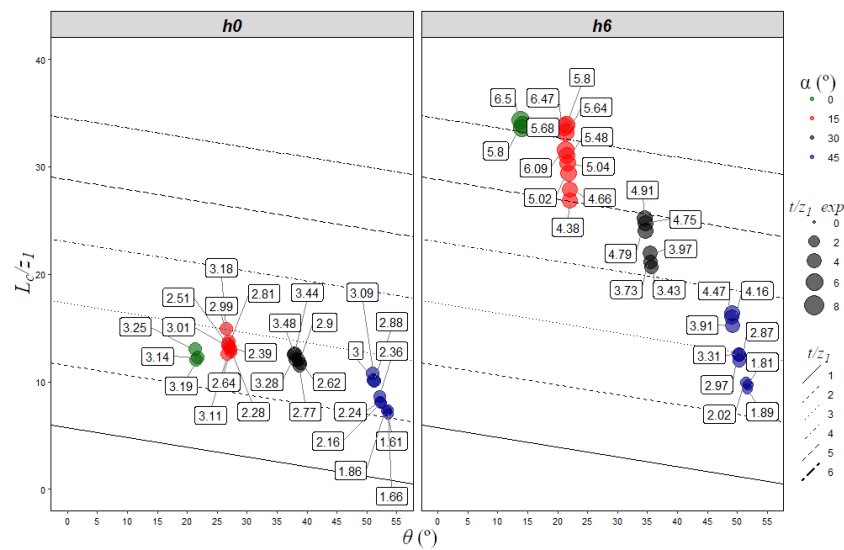


Figure 13. Results obtained for L_c/z_1 with the Equation (2) for several values of t/z_1 and impingement angle (θ). The experimental value of t/z_1 is indicated next to each point (without water cushion, h_0 , and with water cushion, h_6).

3.3. Length of the Erosion Basin

The size of the limit erosion basin was defined by parameters A and B , maximum length and width, respectively, at the level of the sandy bed, 500 mm above the bottom of the testing channel. However, the contour corresponding to the 500 mm height is sometimes open, probably due to the effect of the boundary conditions imposed by the walls of the channel and the flip bucket itself. In order to overcome this difficulty, alternative parameters a and b were considered, with the same meaning as the previous A and B , but defined at the height of 400 mm. It is the highest contour of the erosion hole that is closed in all the tests, which seems to indicate that the effect of the boundary conditions is irrelevant or null at that level (Figure 14).

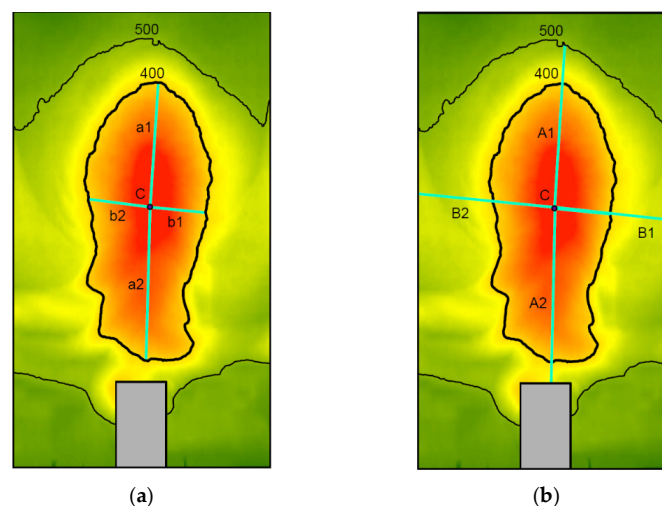


Figure 14. (a) For contour line at height of 400 mm is the limit scour hole semi-axis from the maximum scour point to the furthest downstream and upstream point in the direction of flow, respectively, a_1 and a_2 . In transverse direction to the flow from the maximum scour point towards the furthest point towards are the hydraulic right (b_1) and hydraulic left (b_2). (b) For contour line at the height of 500 mm is the semi-axis in the direction of flow from the maximum scour point to the furthest downstream and upstream point, respectively, A_1 and A_2 ; semi-axis length in the transverse direction to the flow from the maximum scour point is towards the furthest point towards the hydraulic right and left, respectively B_1 and B_2 .

Furthermore, while the jet was aligned with the axis of the spillway, positioned in the middle of the experimental channel and the sand uniformly distributed, it was observed that the main axis in the longitudinal direction was deviated. This phenomenon may be due to the presence of small imperfections in the physical model that are difficult to detect, which can cause a certain asymmetry in the real behavior. In addition, the test channel has a large lateral observation window, so the roughness of their lateral walls is different. This introduces a real asymmetry that could be the main cause of the asymmetry observed in some of the tests. For this reason, the presence of the scour hole with longitudinal axes in the direction of the channel, not rectangular, was resolved by dividing the central axis into two parts: a_1 and a_2 , which are obtained by joining the point of maximum erosion with the level curve of 400 mm in the two furthest points; the same geometric criterion was applied to the transverse axis to obtain b_1 and b_2 . The results obtained with the proposed geometric criterion were compared with the results obtained from applying the morphometric theory of lakes [52] that defines the parameters L_{max} , B_{max} , L_e , and B_e . Figure 15 represents the application of the two criteria to a specific case. The results obtained with both techniques were quite similar. Comparing the values of a , obtained from the sum of a_1 and a_2 , with L_{max} , and the values of b , equal to the sum of b_1 and b_2 , with B_{max} , the MRE was around 2%, so it was finally decided to maintain the geometric criterion here proposed (Figure 16).

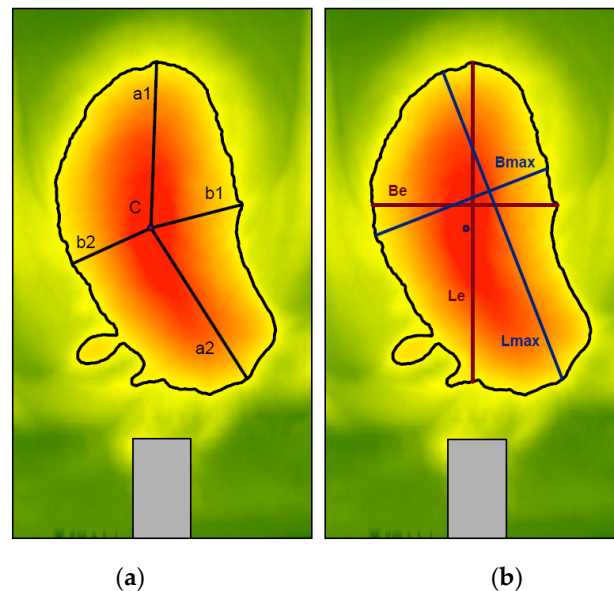


Figure 15. (a) Scour hole axes according to the criterion here proposed. (b) According to the morphometric criterion used in lakes: L_{max} is the line that connects the two points of the lakeshore that are farthest away, B_{max} is the line perpendicular to L_{max} that connects the two most distant points of the shore, L_e is the line that connects the two points of the shore of the lake that are farthest in the direction of the current, B_e is the line perpendicular to L_e that connects the two most distant points. In flow direction, the joining of the point of maximum erosion with the contour level of 400 mm in the two furthest points is given by a_1 and a_2 ; in cross direction, the joining of the point of maximum erosion with the contour level of 400 mm in the two furthest points is given by b_1 and b_2 .

Once the parameters a_1 , a_2 , b_1 , and b_2 were measured, A_1 , A_2 , B_1 , and B_2 were determined by linear extrapolation to the 500 mm curve. To verify that the extrapolation was acceptable, we first selected the tests that presented the 500 mm contour closed and determined directly the axes A_1 , A_2 , B_1 , and B_2 (Table 6). These experimental values were then compared with those obtained by extrapolation, and the error was calculated. The MRE did not exceed 15.22%. Taking into account the uncertainties of the erosion process, the extrapolation was considered acceptable.

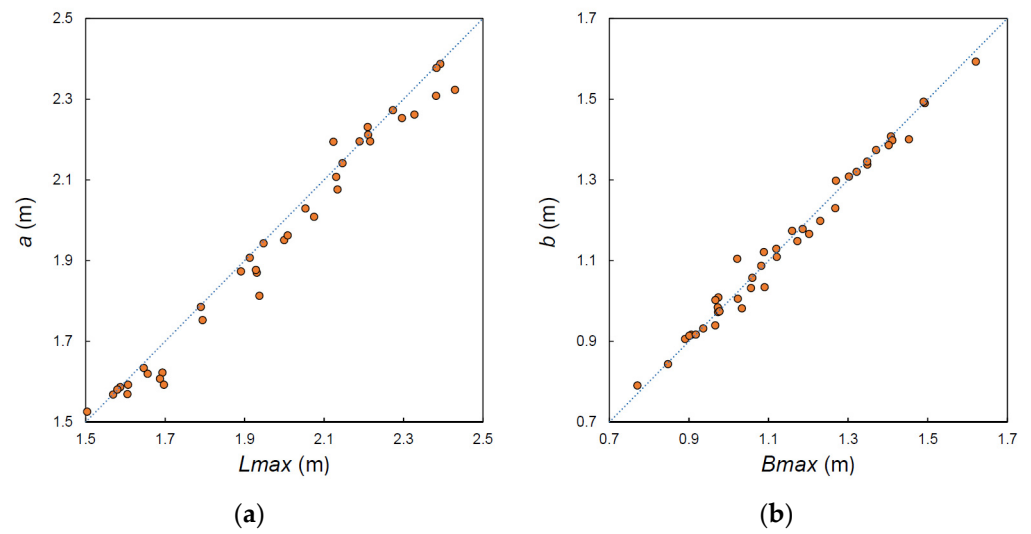


Figure 16. (a) Comparison of parameters a and L_{max} ; (b) b and B_{max} .

Table 6. Absolute and relative errors between extrapolated and measured values and mean absolute and corresponding relative mean error of: (a) axis A_1 , (b) axis A_2 , (c) axis B_1 , and (d) axis B_2 .

(a)					
Practice	A_1 extr	A_1 exp	AE (m)	RE	
A4_h0_17	0.891	0.895	0.004	0.005	
A4_h0_18	1.035	1.027	0.008	0.007	
A4_h0_18	0.983	0.974	0.008	0.009	
A4_h6_17	0.873	1.085	0.211	0.195	
A4_h6_18	0.991	0.916	0.075	0.082	
A4_h6_20	1.027	1.035	0.007	0.007	
B3_h0_20	1.158	1.210	0.051	0.042	
B3_h6_17	1.026	0.982	0.044	0.045	
B4_h6_18	0.989	1.052	0.063	0.060	
B4_h6_20	1.062	1.095	0.032	0.029	
C4_h0_17	1.032	1.001	0.031	0.031	
C4_h0_20	1.058	1.120	0.062	0.056	
C4_h6_17	0.920	0.878	0.042	0.048	
C4_h6_20	0.901	0.931	0.030	0.033	
			MAE _v	0.048	
			MRE _v		0.046
(b)					
Practice	A_2 extr	A_2 exp	AE (m)	RE	
A4_h0_17	1.163	1.244	0.081	0.065	
A4_h0_18	1.075	1.114	0.038	0.034	
A4_h0_18	1.285	1.516	0.231	0.152	
A4_h6_17	1.082	1.137	0.056	0.049	
A4_h6_18	1.042	1.280	0.238	0.186	
A4_h6_20	1.067	1.189	0.122	0.102	
B3_h0_20	1.468	1.519	0.051	0.034	
B3_h6_17	2.008	1.525	0.483	0.316	
B4_h6_18	1.027	0.997	0.030	0.030	
B4_h6_20	1.137	1.764	0.627	0.356	
C4_h0_17	1.426	1.245	0.181	0.145	
C4_h0_20	1.518	1.559	0.042	0.027	
C4_h6_17	1.650	1.517	0.133	0.088	
C4_h6_20	1.468	1.200	0.269	0.224	
			MAE _v	0.184	
			MRE _v		0.129

Table 6. *Cont.*

(c)				
Practice	B ₁ extr	B ₁ exp	AE (m)	RE
A4_h0_17	0.787	0.795	0.009	0.011
A4_h0_18	0.810	0.830	0.020	0.024
A4_h0_18	0.915	0.813	0.102	0.125
A4_h6_17	0.725	0.753	0.027	0.036
A4_h6_18	0.914	0.844	0.070	0.083
A4_h6_20	0.930	0.884	0.046	0.052
B3_h0_20	0.930	1.256	0.326	0.259
B3_h6_17	0.752	0.846	0.094	0.111
B4_h6_18	0.736	0.734	0.003	0.004
B4_h6_20	0.861	0.837	0.023	0.028
C4_h0_17	1.033	1.087	0.054	0.050
C4_h0_20	0.768	0.809	0.041	0.051
C4_h6_17	0.579	0.694	0.115	0.166
C4_h6_20	0.752	1.110	0.358	0.322
			MAEv	
			MREv	0.094
(d)				
Practice	B ₂ extr	B ₂ exp	AE (m)	RE
A4_h0_17	0.900	0.979	0.079	0.080
A4_h0_18	0.989	1.147	0.159	0.139
A4_h0_18	0.999	1.113	0.114	0.103
A4_h6_17	0.877	1.085	0.208	0.191
A4_h6_18	0.892	1.136	0.244	0.215
A4_h6_20	0.910	0.993	0.083	0.083
B3_h0_20	0.794	0.921	0.127	0.138
B3_h6_17	0.765	0.991	0.226	0.228
B4_h6_18	0.772	1.043	0.271	0.260
B4_h6_20	0.967	1.206	0.239	0.198
C4_h0_17	0.708	0.813	0.105	0.129
C4_h0_20	1.221	1.343	0.123	0.091
C4_h6_17	0.744	0.920	0.175	0.191
C4_h6_20	0.652	0.712	0.060	0.084
			MAEv	
			MREv	0.152

It was observed that the longitudinal axis (*A*) decreases when the flip angle (α) increases (Figure 17), in agreement with the fact that erosion develops more vertically for high angles and progresses downstream for lower angles, which result in a longer scour hole.

The values of *A*₁ and *A*₂ were considered to calculate the length of the major axis *A*, and a linear regression type adjustment was performed. Cases where the scour hole reached the foot of the trampoline were excluded, which could distort the result. The calibration and validation sets were differentiated. The formulas obtained for *A*₁ and *A*₂ (Equations (4) and (5)), respectively, present an R² of 0.984 and 0.980. Considering the validation data, for parameter *A*₁ the MAEv is 0.13 m, and the MREv is 10.70%, and for *A*₂, the MAEv is 0.12 m, and the MREv is 8.40%. The value of *A* (Equation (6)) results from the sum of *A*₁ and *A*₂ and presents a MAE equal to 0.19 m and an MRE of 7.40%.

$$A_1 = (0.18 t + 1.30 \cos^2 \theta) \tag{4}$$

$$A_2 = (0.85 t + 2.26 \cos^2 \theta) \tag{5}$$

$$A = A_1 + A_2 \tag{6}$$

where t is the scour depth and θ is the impingement angle.

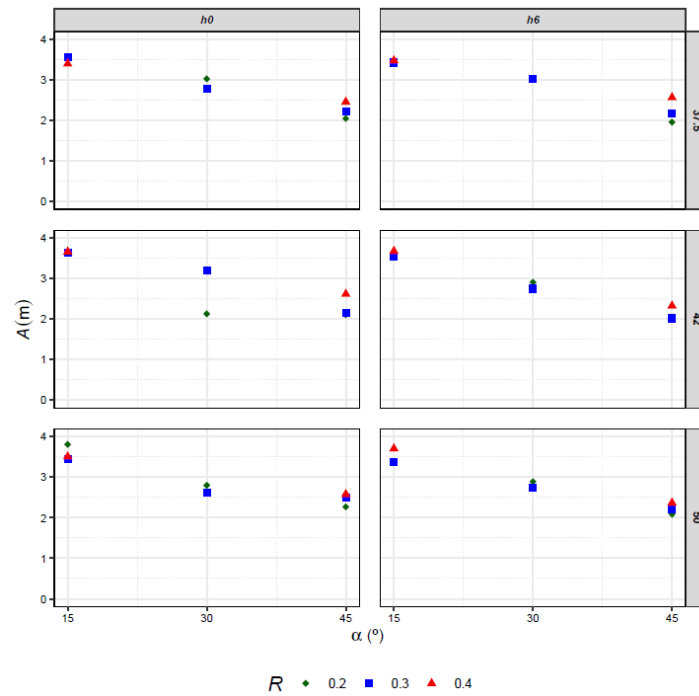


Figure 17. Evolution of the maximum length (A) of the scour hole with the flip angle (α), separating the data by the height water cushion (0.00 m or 0.06 m; columns), by the flow rate (37.5 L/s, 42 L/s, 50 L/s; lines), and by the radius (0.2, 0.3, 0.4 m; shape and color).

It can be observed that Equation (4) has a good correspondence with the experimental values (Figure 18) and that parameter A_1 increases when $\cos^2\theta$ increases, confirming that the scour hole lengthens when the impingement angle (θ) decreases. Equation (5) fits the experimental results quite well for cases that have a radius other than 0.40 m (Figure 19).

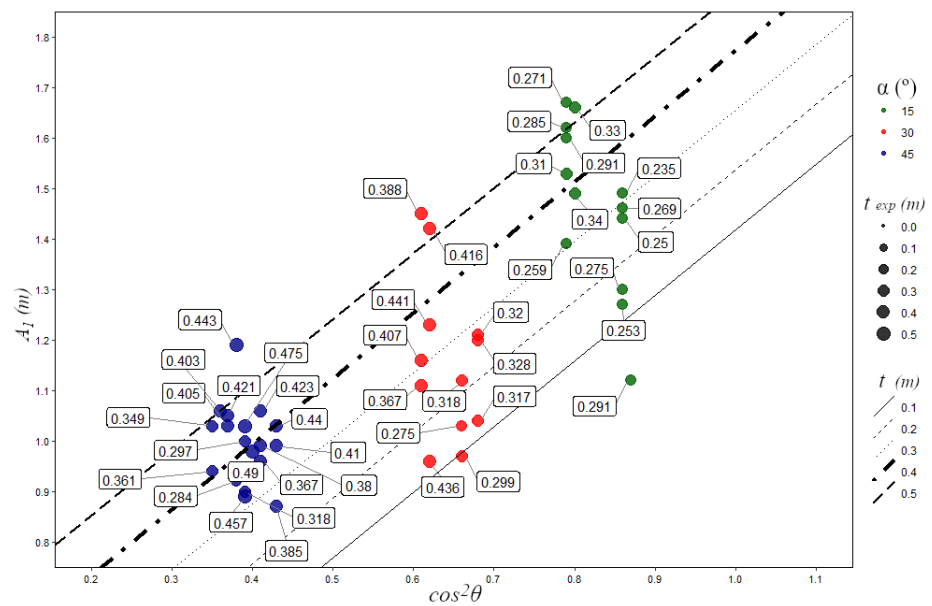


Figure 18. Lines obtained with Equation (4) for various values of scour depth (t), covering the range of experimental values, including in the graph (A_1 ; $\cos^2\theta$) the experimental points with the corresponding value of t .

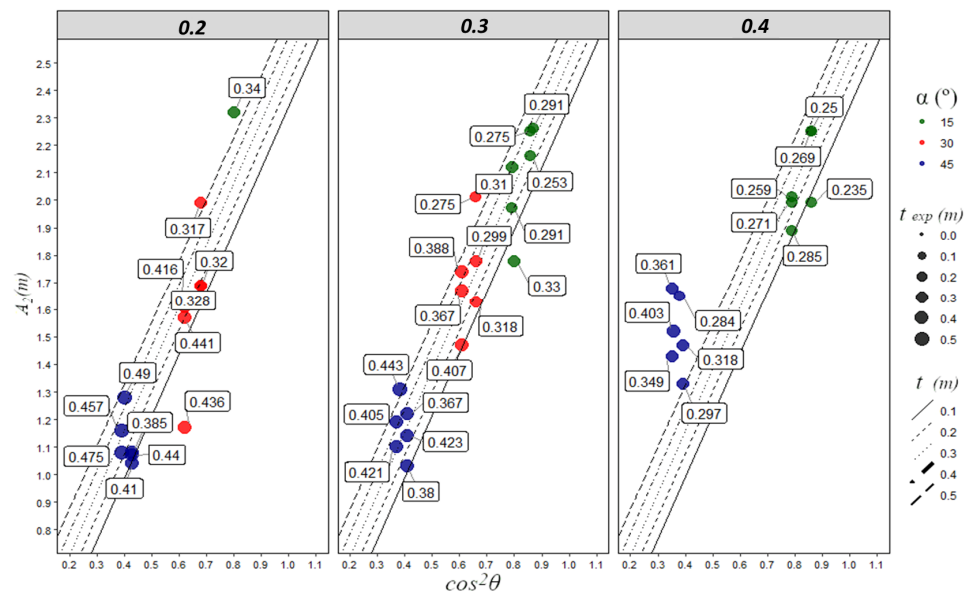


Figure 19. Lines obtained with Equation (4) for various values of scour depth (t), covering the range of experimental values, including in the graph ($A_2; \cos^2\theta$) the experimental points with the corresponding value of t and separating the data as a function of the radius R .

3.4. Erosion Basin Shape

The shape of the limit scour hole was characterized by the relationship between its longitudinal and transverse axes A/B , which we call the circularity index. This index would adopt the unit value for a perfect circle, and its value increases as the shape becomes more elongated. Tests have clearly shown that for a high flip angle (45°), the scour hole has a rounded or quasi-circular shape, while it is more elongated for smaller flip angles. Furthermore, it is observed that the circularity index A/B increases when the flip angle (α) decreases (Figure 20). When the scour hole reaches the foot of the flip bucket, its shape is affected by this obstacle. Therefore, these cases were not considered for the regression adjustment.

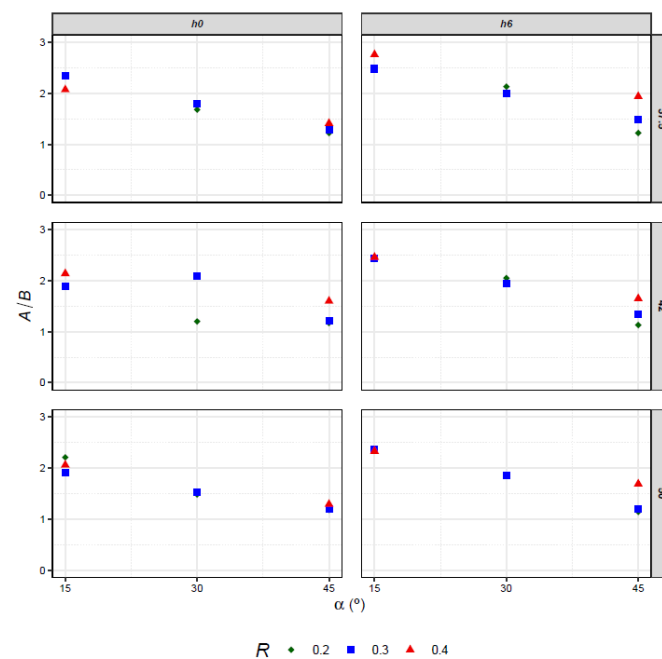


Figure 20. Evolution of the circularity index A/B with the flip angle (α), separating in two columns the cases without water cushion h_0 from those with water cushion h_6 and separating in three rows the test flows rates (37.5 L/s, 42 L/s, 50 L/s). Radius (R) is indicated by color and shape.

The circularity index can be obtained as a/b or A/B , since homologous axes are homothetic. For the determination of the formula of the circularity index, a linear regression type adjustment was performed. The formula obtained (Equation (7)) has an $R^2 = 0.985$. Applying the formula to validation cases results in an MAEv of 0.15 m and an MREv of 8.70%.

$$\frac{A}{B} = \left(0.49 \frac{R}{t} + 1.73 \cos \theta \right) \tag{7}$$

where t is the scour depth, θ is the impingement angle, and R the radius of flip bucket.

It can be observed that Equation (7) has a good correspondence with the experimental values (Figure 21). The parameter A/B increases when the $\cos \theta$ increases, as expected due to the fact that the scour hole lengthens when the impingement angle (θ) decreases.

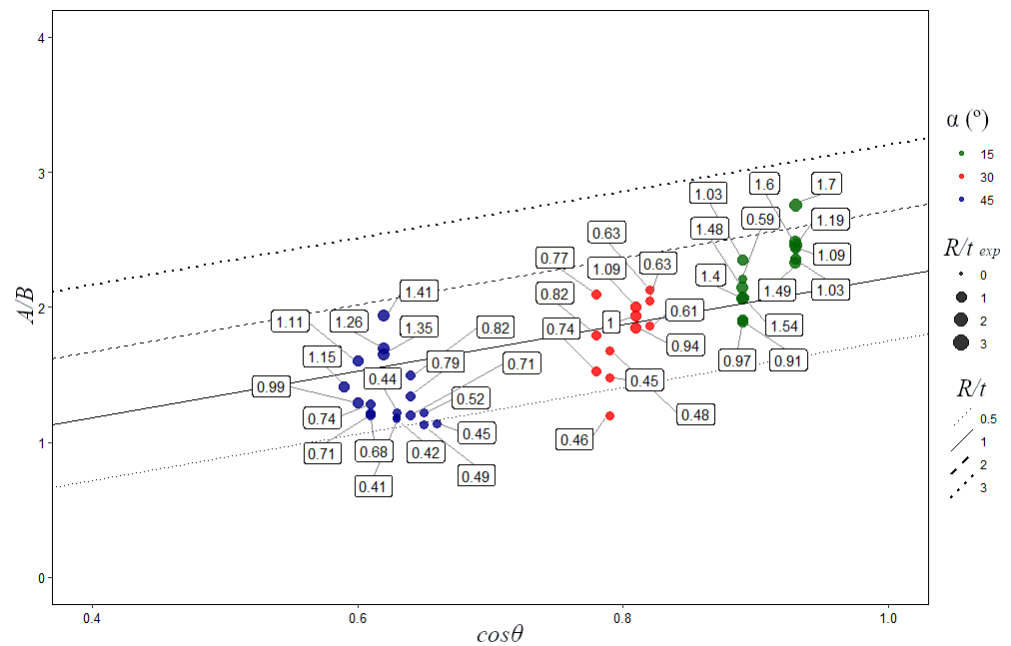


Figure 21. Lines obtained with equation for various values of R/t , covering the range of experimental values, including in the graph $(A/B; \cos \theta)$ the experimental points with the corresponding value of R/t and separating the data as a function of the flip angle (α).

3.5. Procedure for Estimating the Location, the Size, and the Shape of the Erosion Basin

Based on the formulas described above, a simple procedure is proposed to characterize the limit erosion basin’s location, shape, and size that takes into account the geometric parameters that define a cylindrical flip bucket (Figure 22). The necessary data are (a) the scour depth (t), which the designer can estimate by one of the available formulas, to be chosen by the designer (for example Equation (1)); (b) the radius of flip bucket (R); (c) the flip angle (α); (d) the vertical distance from the lip of the flip bucket to the level of the reservoir (z_0); (e) the vertical distance from the lip of the flip bucket to the surface of the water downstream (z_1); and (f) the impingement angle of incidence (θ), which can be determined with equations present in the literature [50].

The process has the following steps:

Step 1: Once the scour depth (t) is known, we estimate L_c , the distance on the horizontal plane from the foot of the flip bucket to point C, where the erosion is maximum. The designer can use Equations (2) or (3) for this.

Step 2: Assuming that two tangent semi-ellipses approximate the shape of the scour hole with a common transverse axis, we proceed by determining the two longitudinal semi-axes A_1 and A_2 (Equations (4) and (5)). The total length of the longitudinal axis A is obtained from the sum of A_1 and A_2 .

Step 3: Check if $L_c > A_2$. If the answer is positive, it should be expected that the limit scour hole would not affect the base of the flip bucket.

Step 4: The circularity index A/B is determined by Equation (7).

Step 5: Once determined, A and the ratio A/B , the axis B can immediately be obtained.

In order to validate the procedure, the cases used for the validation of the formulas, not for their calibration, were considered. The limit scour holes resulting from the application of the proposed procedure were drawn and compared with the experimental data (Figure 23). Table 7 summarizes the differences between the experimental and calculated data quantified as mean absolute error (MAEv) and mean relative error (MREv) for all the studied parameters. It can be observed that the MREv is, for all the dimensions that define the limit scour hole in its shape and size, less than 10%, while for the L_c parameter, the MREv is less than 17.5%. It should be noted that this procedure concerns a flip bucket with a certain width, so that width and shape cannot be extrapolated to other cases. However, the estimation of length and position of the limit erosion basin are the most relevant parameters from a design or safety point of view.

A question of great importance is to know if erosion might affect the structure, that is, if the parameter A_2 is greater than the parameter L_c ; in this circumstance, it should be expected that the erosion would affect the flip bucket. Equation (5) (calculation of A_2) is applied using the validation tests (Table 8). It is observed that in cases where the 500 mm contour line touches the trampoline (Figure 24), the value of A_{2_cal} must be greater than the mean value of $\overline{L_c}$ calculated with Equations (2) and (3); only in two cases (A4_h0_17; B4_h0_18) the value of A_{2_cal} is not greater than the mean value of $\overline{L_c}$, although the 500 mm contour line touches the trampoline. In any case, this observation further validates the proposed formula because it is correct ten times out of twelve.

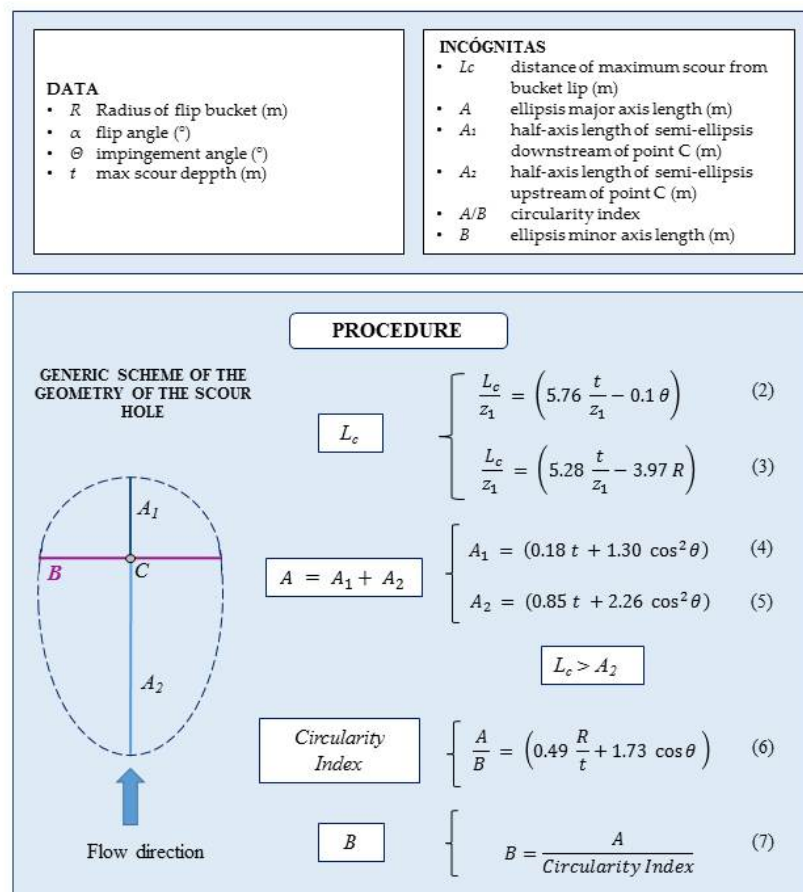


Figure 22. Procedure for the estimation of the position, size, and shape of the limit scour hole.

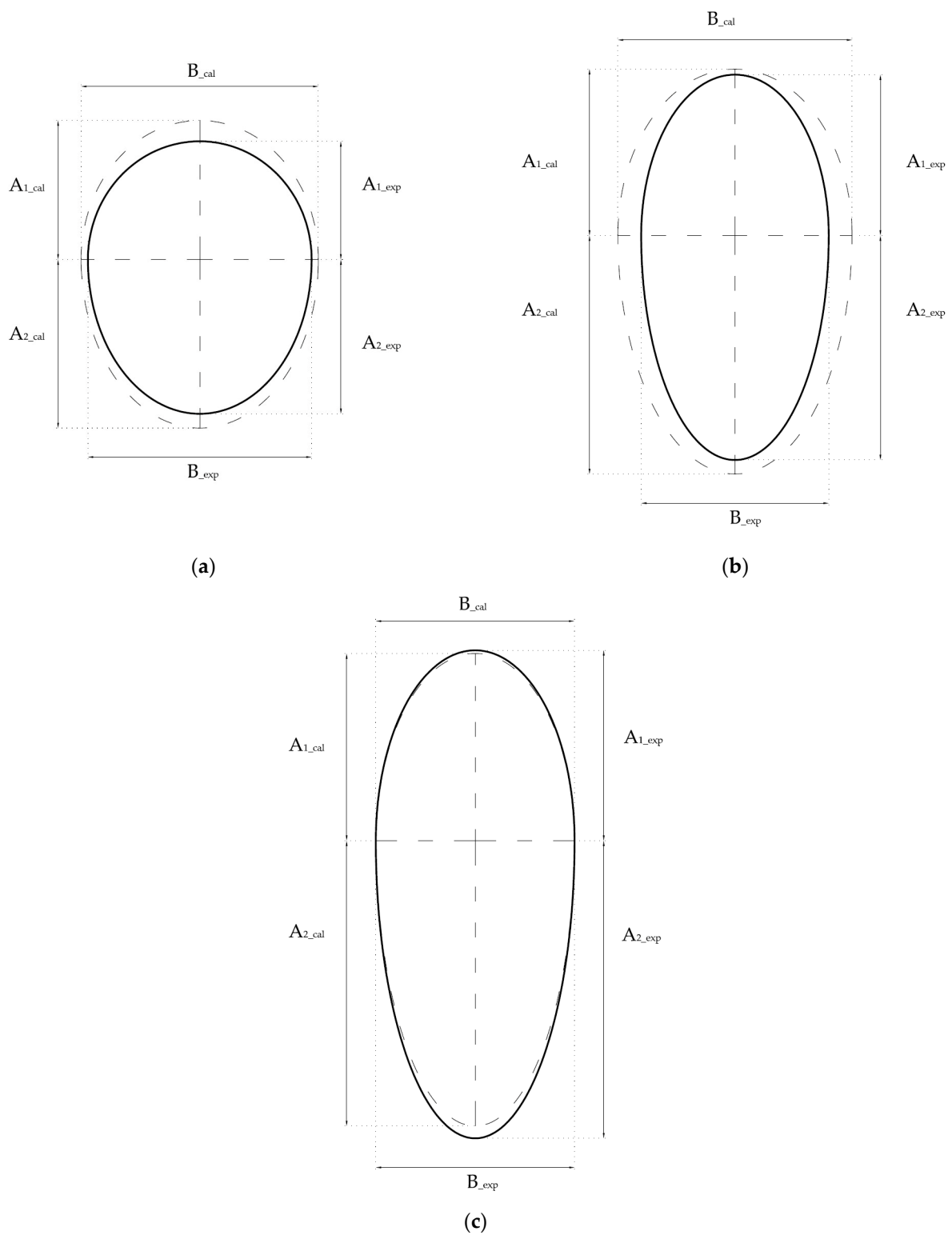


Figure 23. Comparison between the shape, size, and position of limit scour hole obtained experimentally (continuous line) and those determined by the proposed procedure (dashed line). Some examples: (a) $R = 0.2$ m, $\alpha = 45^\circ$, $Q = 37.5$ L/s and without water cushion. (b) $R = 0.2$ m, $\alpha = 30^\circ$, $Q = 50$ L/s and with water cushion of 0.06 m. (c) $R = 0.4$ m, $\alpha = 15^\circ$, $Q = 42$ L/s and with water cushion of 0.06 m.

Table 7. MAEv and MREv of the calculated parameters of the scour hole taking the measured data as a reference, considering all the validation tests.

Parameter	$L_c(\theta)$ (m)	$L_c(R)$ (m)	A_1 (m)	A_2 (m) (m)	A (m) (m)	A/B	B (m) (m)
MAEv (m)	0.19	0.26	0.126	0.12	0.19	0.15	0.15
MREv (%)	12.76	17.44	10.70	8.40	7.40	8.70	9.90

Table 8. Comparison of the value of A_2 , calculated with Equation (5), with the experimental and calculated values of L_c for validation tests.

Validation Test	t (m)	$\cos^2\theta$	A_{2_exp} (m)	A_{2_cal} (m)	L_{c_exp} (m)	$L_c(\theta)$ (m)	$L_c(R)$ (m)	Reached Trampoline	$A_{2_cal} > \overline{L_c}$
A3_h0_20	0.441	0.62	1.568	1.785	1.594	2.061	2.228	no	no
A3_h6_18	0.320	0.68	1.694	1.800	1.607	1.612	1.637	yes	yes
A4_h0_17	0.457	0.39	1.163	1.271	1.596	1.819	2.287	yes	no
A4_h6_18	0.410	0.43	1.042	1.314	1.572	1.877	2.087	no	no
B2_h0_17	0.291	0.79	1.970	2.037	1.429	1.377	1.405	yes	yes
B2_h6_20	0.291	0.87	2.262	2.202	1.704	1.568	1.477	yes	yes
B3_h0_17	0.367	0.61	1.666	1.681	1.641	1.569	1.771	yes	=
B3_h6_20	0.318	0.66	1.627	1.769	1.756	1.548	1.584	yes	yes
B4_h0_18	0.421	0.37	1.098	1.202	1.514	1.443	1.999	yes	no
B4_h6_17	0.367	0.41	1.216	1.228	1.594	1.469	1.786	no	no
C2_h0_20	0.285	0.79	1.885	2.033	1.507	1.334	1.324	yes	yes
C2_h6_18	0.250	0.86	2.246	2.154	1.497	1.322	1.235	yes	yes

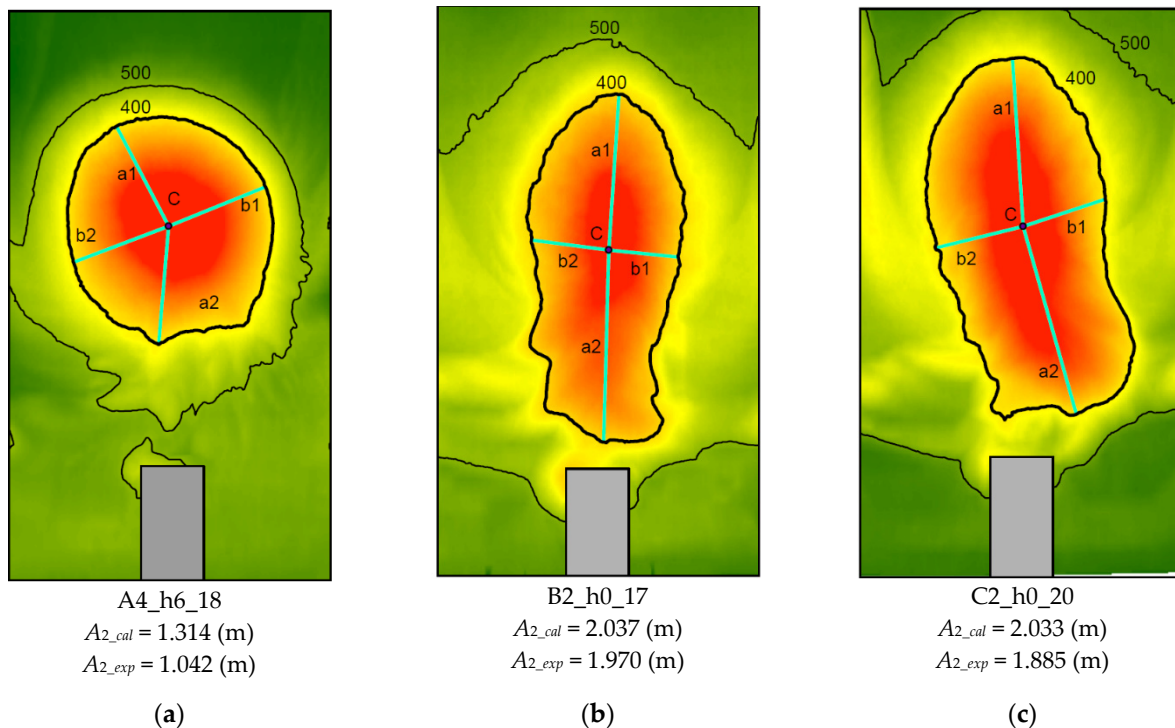


Figure 24. Digital terrain model for some tests, with contour lines at 400 mm and 500 mm, and longitudinal (a_1 and a_2) and transverse axes (b_1 and b_2) closed on curve line 400 mm, for three tests: (a) A4_h6_18 ($R = 0.2$ m, $\alpha = 45^\circ$, with a water cushion of 0.06 m and $Q = 42.00$ L/s), (b) B2_h0_17 ($R = 0.3$ m, $\alpha = 15^\circ$, without a water cushion and $Q = 37.50$ L/s), (c) C2_h0_20 ($R = 0.4$ m, $\alpha = 15^\circ$, without a water cushion and $Q = 50.00$ L/s). For every test, the calculated and measured value of A_2 (the semi-axis length in the direction of flow from the maximum scour point to the furthest upstream point) is provided.

A different shape and orientation of the limit scour hole can be seen in the same Figure 24; in particular, the shape can be more circular or more elliptical, and the orientation can be more leftward or rightward. This can be explained considering the flip angle; in fact, when this angle is small, the horizontal component of the jet velocity is greater than the vertical, causing greater erosion in the longitudinal direction; it means a greater amount of energy is dissipated in direction of the flow. Regarding shape, the dimension in the direction of the flow is the most relevant characteristic as the dimension transversal to the flow depends on the width of the spillway, which remains constant in this study. For the orientation to the left or right, there is not a plausible explanation. An explication of these changes of orientation can be determined by random small imperfections and a not perfect symmetry of the facility given by the different naturalness of the experimental channel walls, which would justify that the orientation does not maintain a clear pattern.

3.6. Limitations of the Present Study

This study provides the designer or engineer with one more tool to design or evaluate the safety of a dam; nevertheless, it has some limitations:

- The height of the spillway is constant, so it has not allowed us to obtain a formula in order to estimate the depth of erosion depending on the flow and the geometric characteristics of the spillway; one of the formulas provided by any other author can be used for this purpose;
- The spillway width is constant, so it has not allowed us to provide a direct formula for the estimation of the total width of the limit scour hole;
- A wider test channel would reduce the effect of the walls, which are most likely the reason for the deviations observed in the limit scour hole.

Depending on the particular characteristics of the case, the preliminary or detailed design phase and the safety study, and the available budget, the responsible engineer will judge the tool of this study sufficient or not. For example, if it is an embankment dam founded on alluvial material with a significant thickness, a better approximation can be expected than if the foundation of the dam is made of competent rock.

In any case, this study can be useful in order to make a simple estimation of the limit erosion basin when making decisions about the design itself or about the need of undertaking more detailed work.

4. Conclusions

The designer should be aware of the significant influence of the design of the flip bucket on the position, size, and shape of the limit erosion basin.

For the first time, the influence of flip bucket design, flip angle, and radius on the position, dimensions, and shape of the limit erosion basin has been investigated. This study provides some formulas and a procedure to estimate that position, size, and shape of the limit erosion basin. In addition, this work reveals and quantifies the influence of the lip angle on the formation of the limit erosion basin, and it evinces a surprising relationship between the radius of the flip bucket and the depth of the scour hole.

The practical utility of these results is immediate, since the designer can adapt the design of the flip bucket to avoid affecting auxiliary structure, the hillsides, or the spillway and dam itself, proceeding from the safety side as a limit erosion basin is handled.

The flip angle and also the radius chosen in the design stage, together with the flow discharge and configuration of the riverbed, determine the depth, length, width, position, and shape of the limit erosion basin. Establishing a priori the position and size of the scour hole allows to control the potential affection to appurtenant works and the flip bucket itself. The same information is useful for the safety assessment of dams in operation when the limit erosion hole has not yet fully developed.

A methodology is here proposed to estimate the position, size, and shape of the limit scour hole, depending on the geometric characteristics of the flip bucket. Whether or not the estimated size is reached depends on the geological/geotechnical characteristics

of the impact area. The main conclusions of the research can be summarized in the following points:

- Increasing the radius of the flip bucket allows a reduction in the depth of the scour hole. Although the cost of the structure is higher for a greater radius, this extra cost might in some cases be justified for the extra safety level achieved.
- The greater the flip angle is, in the range of tested angles, 15° to 45° , the greater the depth of erosion is.
- Scour hole is longer in the riverbed direction and less deep for low flip angles.
- For the length of flip bucket tested, the scour hole is quasi-circular for a flip angle of 45° and more elongated for lower angles. However, the influence of the lip length is evident, so a different shape should be expected for different lip lengths.
- The plan position of the point where the depth erosion is maximum moves away from the flip bucket with increasing flip angles between 0° and 30° . However, it is nearer the structure for a flip angle of 45° . Two opposite effects might explain this fact: increasing the angle increases the launch scope, up to 45° , but a greater angle of incidence makes the erosion more vertical, so the scour hole develops less in the direction of the riverbed and more in depth.
- Empirical formulas were derived from the experimental data to estimate the position, size and shape of the scour hole. However, it should be noted that a different width, and so shape, should be expected for different lengths of the flip bucket lip, which is a parameter not considered in this experimental research. More tests are needed with different lip lengths.
- A methodology is proposed, using the above mentioned formulas, to estimate position, size, and shape of the scour hole, which was fitted to a combination of two semi-ellipses.
- The proposed methodology was used with success to determine whether the scour hole is likely to affect the flip bucket structure, comparing the length of the scour hole upstream of the point where the depth is maximum with the distance from that point to the flip bucket. If the scour hole overlaps with the structure, affection is likely to occur.

Author Contributions: Conceptualization, M.Á.T.; methodology, M.Á.T. and R.P.; validation, R.P.; formal analysis, R.P.; investigation, R.P.; resources, M.Á.T.; data curation, R.P.; writing—original draft preparation, R.P.; writing—review and editing, M.Á.T.; visualization, R.P.; supervision, M.Á.T.; project administration, M.Á.T. All authors have read and agreed to the published version of the manuscript.

Funding: This research received no external funding.

Institutional Review Board Statement: Not applicable.

Informed Consent Statement: Not applicable.

Data Availability Statement: The data relating to this work are collected in Raffaella Pellegrino's doctoral thesis available in the library of Universidad Politécnica de Madrid.

Acknowledgments: We are grateful to the members of the research group SERPA-Dam Safety Research for the support provided.

Conflicts of Interest: The authors declare no conflict of interest.

Abbreviations

The following abbreviations are used in this paper:

A	total length of the limit scour hole in the river longitudinal direction
A/B	circularity index
A_1	semi-axis length in the direction of flow from the maximum scour point to the furthest downstream point

A_2	semi-axis length in the direction of flow from the maximum scour point to the furthest upstream point
AR	absolute error
B	total width of the limit scour hole
B_1	semi-axis length in the transverse direction to the flow from the maximum scour point towards the furthest point towards the hydraulic right
B_2	semi-axis length in the transverse direction to the flow from the maximum scour point towards the furthest point towards the hydraulic left
D	total scour depth
D_{exp}	experimental total scour depth
D_{cal}	calculated total scour depth
d_{50}	grain diameter at 50% of weight
d_{90}	grain diameter at 90% of weight
H	total head (distance between upstream and downstream water level)
h_2	tailwater depth (downstream water level)
L_c	distance of maximum scour from bucket lip
MAE	mean absolute error
MRE	mean relative error
Q	flow rate
q	unit flow rate
R	radius of flip bucket
RE	relative error
T	scour depth
z_1	distance from the flip bucket's lip to the downstream water level
z_0	distance between flip bucket's lip and upstream water level
z_p	distance from the flip bucket's lip to the ground
α	flip angle
θ	impingement jet angle

References

- Pfister, M.; Schleiss, A.J. Ski Jumps, Jets and Plunge Pools. In *Energy Dissipation in Hydraulic Structures*; Chanson, H., Ed.; IAHR Monograph; CRC Press, Taylor & Francis Group: Leiden, The Netherlands, 2015.
- Schoklitsch, A. *Kolkbildung Unter Ueberfallstrahlen*; Berlin, Germany Verlag Nicht Ermittlbar; 1932.
- Veronese, A. Erosioni di Fondo a Valle di Uno Scarico. *Annale dei Lavori Pubblici* **1937**, *75*, 717–176.
- United States Bureau of Reclamation. *Design of Small Dams*; US Department of the Interior, Bureau of Reclamation: Washington, DC, USA, 1987.
- Yildiz, D.; Üzücek, E. Prediction of scour depth from free falling flip bucket jets. *Int. Water Power Dam Constr.* **1994**, *46*, 50–56.
- Chanson, H.; Gonzalez, C.A. Physical modelling and scale effects of air-water flows on stepped spillways. *J. Zhejiang Univ.-Sci.* **2005**, *6*, 243–250.
- Jian-ming, Y.; Jian-hua, W. Numerical simulation of scouring process under spillway. *J. Hydrodyn.* **2001**, *4*, 55–59.
- Heller, V.; Hager, W.H.; Minor, H. Ski jump hydraulics. *J. Hydraul. Eng.* **2005**, *131*, 347–355.
- Schmocker, L.; Pfister, M.; Hager, W.H. Aeration characteristics of ski jump jets. *J. Hydraul. Eng.* **2008**, *134*, 90–97. [[CrossRef](#)]
- Azmathullah, H.M.; Deo, M.C.; Deolalikar, P.B. Neural networks for estimation of scour downstream of a ski-jump bucket. *J. Hydraul. Eng.* **2005**, *131*, 898–908.
- Lee, T.L. Neural network modeling for estimation of scour depth around bridge piers. *J. Hydrodyn.* **2007**, *19*, 378–386. [[CrossRef](#)]
- Damle, P.M.; Venkatraman, C.P.; Desai, S.C. *Evaluation of Scour Below Ski-Jump Buckets of Spillways*; CWPRS Golden Jubilee Symposia, 1966; Available online: https://scholar.google.com.hk/scholar?hl=zh-CN&as_sdt=0%2C5&q=Evaluation+of+Scour+Below+Ski-Jump+Buckets+of+Spillways&btnG= (accessed on 12 June 2023).
- Rubinstein, G.L. Laboratory investigation of local erosion on channel beds below high overflow dams. In *Transactions of Coordination Conferences on Hydraulic Engineering. 1ss. VII, Conference on Hydraulics of High Head Water Discharge Structures*; Gosenergoizdat: Moscow, Russia, 1963.
- Yuditskii, G.A. *Experimental Prediction of Rock Bed Scour Below a Ski-Jump Spillway Dam*; 81–90. Jerusalem: IPST. Trans. Vedeneev All-Union Scientific Research Institute of Hydraulic Engineering, 1971; Available online: https://scholar.google.com.hk/scholar?hl=zh-CN&as_sdt=0%2C5&q=Experimental+Prediction+of+Rock+Bed+Scour+Below+a+Ski-Jump+Spillway+Dam&btnG= (accessed on 12 June 2023).

15. Mirskhulava, T. Mechanism and computation of local and general scour in non-cohesive, cohesive soils and rock beds. In Proceedings of the 12th Congress of the IAHR, Fort Collins, CO, USA, 11–14 September 1967; Volume 3, pp. 169–176.
16. Zvorykin, K.A.; Kouznetsov, N.V.; Akhmedov, T.K. Scour of Rock bed by a jet spilling from a deflecting bucket of an overflow dam. In Proceedings of the 16th IAHR Congress, São Paulo, Brazil, 27 July–1 August 1975; Volume 2.
17. Doddiah, D.; Albertson, M.L.; Thomas, R. Scour from jet. In Proceedings of the 5th IAHR Congress, Minneapolis, MN, USA, 1–4 September 1953.
18. Ervine, D.A. The entrainment of air in water. *Water Power Dam Constr.* **1976**, *28*, 27–30.
19. Canepa, S.; Hager, W.H. Effect of jet air content on plunge pool scour. *J. Hydraul. Eng.* **2003**, *129*, 358–365.
20. Pagliara, S.; Hager, W.H.; Minor, H. Hydraulics of plane plunge pool scour. *J. Hydraul. Eng.* **2006**, *132*, 450–461. [[CrossRef](#)]
21. Castillo, L.G.; Carrillo, J.M.; Blázquez, A. Plunge pool dynamic pressures: A temporal analysis in the nappe flow case. *J. Hydraul. Res.* **2015**, *53*, 101–118. [[CrossRef](#)]
22. Castillo, L.G.; Carrillo, J.M. Scour, velocities and pressures evaluations produced by spillway and outlets of dam. *Water* **2016**, *8*, 68. [[CrossRef](#)]
23. Mason, P.J. Scour Downstream of Energy Dissipating Spillways. In *Thesis Submitted for the Degree of Master of Philosophy*; Department of Civil Engineering, City University: London, UK, 1983.
24. Chee, S.P.; Kung, T. Stable profiles of plunge basins. *J. Am. Water Resour. Assoc.* **1971**, *7*, 303–308. [[CrossRef](#)]
25. Pagliara, S.; Dipankar, R.; Palermo, M. 3D plunge pool scour with protection measures. *J. Hydro-Environ. Res.* **2010**, *4*, 225–233. [[CrossRef](#)]
26. Pagliara, S.; Dipankar, R.; Palermo, M. Scour due to crossing jets at fixed vertical angle. *J. Irrig. Drain. Eng.* **2011**, *137*, 49–55. [[CrossRef](#)]
27. Azmathullah, H.M.; Ghani, A.A.B.; Zakaria, N.A. Prediction of scour below flip bucket using soft computing techniques. In Proceedings of the 12th International Conference on enhancement and promotional methods in engineering and science, Hong Kong, China, 30 November–3 December 2009.
28. Sammen, S.S.; Ghorbani, M.A.; Malik, A.; Tikhamarine, Y.; Amirrahmani, M.; Al-Ansari, N.; Chau, K.W. Enhanced artificial neural network with Harris hawks optimization for predicting scour depth downstream of ski-jump spillway. *Appl. Sci.* **2020**, *10*, 5160. [[CrossRef](#)]
29. Castillo, L.G.; Carrillo, J.M. Comparison of methods to estimate the scour downstream of a ski jump. *Int. J. Multiph. Flow* **2017**, *92*, 171–180. [[CrossRef](#)]
30. INCYTH-LHA. *Estudio Sobre Modelo de Aliviadero de la Presa Casa de Piedra, Informe Final*; Laboratorio de Hidráulica Instituto Nacional del Agua: Ezeiza, Argentina, 1982.
31. Eggenberger, W. Die Kolkbildung Bei Einem Überstromen und Bei Der Kombination Überstromen-Unterstromen. Ph.D. Thesis, ETH Zürich, Zurich, Switzerland, 1994.
32. Hartung, W. Die Kolkbildung hinter überstromten wehren im hindblick auf eine beweglich sturzbettgestaltung. *Die Wasser Wirtshaft* **1959**, *49*, 309–313.
33. Franke, P.G. Über kalkbildung und kolkformen. *Oesterreichische Wasserwirtschaft* **1960**, *1*, 11–16.
34. Martins, R. Contribution to the knowledge on the scour action of free jets on rocky river-beds. *11th Inter. Comm. Large Dams Trans.* **1973**, *44*, 799–814.
35. Martins, R. Scouring of rocky riverbeds by free-jet spillways. *Int. Water Power Dam. Constr.* **1975**, *27*, 152–153.
36. Taraimovich, I.I. Deformations of channels below high-head spillways on rock foundations. *Hydrotech. Constr.* **1978**, *12*, 917–923. [[CrossRef](#)]
37. Machado, L.I. *O Sistema de Dissipacao de Energia Proposto para a Barragem de Xingo*; Transactions of the International Symposium on the Layout of Dams in Narrow Gorges ICOLD: Rio de Janeiro, Brazil, 1982.
38. SOFRELEC. *Kamdadji Dam, Niger, 3rd Phase Design Report*; Société FranGaise d’Etudes et de Realisation d’Equipement Electriques: Paris, France, 1980.
39. Kotoulas, D. Das Kolkproblem unter Besonderer Berücksichtigung der Faktoren Zeit und Geschiebemischung im Rahmen der Wildbachverbauung. Ph.D. Thesis, ETH Zurich, Zurich, Switzerland, 1967.
40. Chee, S.P.; Padiyar, P.V. Erosion at the base of flip buckets. *Eng. J.* **1969**, *52*, 22–24.
41. Bisaz, E.; Tschopp, J. Profundidad de erosión al pie de un vertedero para la aplicación de corrección de arroyos en quebradas empinadas. In Proceedings of the Fifth Congreso Latinoamericano de Hidraulica, Lima (IAHR), Peru, 23–28 October 1972.
42. Jaeger, C. *Engineering Fluid Mechanics*; Blackie and Sons Ltd.: London, UK, 1956.
43. Mason, P.J.; Arumugam, K. Free jet scour below dams and flip buckets. *J. Hydraul. Eng.* **1985**, *111*, 220–235. [[CrossRef](#)]
44. Ghodsian, M.; Mehraein, M.; Ranjbar, H.R. Local scour due to free fall jets in non-uniform sediment. *Sci. Iran.* **2012**, *19*, 1437–1444. [[CrossRef](#)]
45. Kumar, C.; Sreeja, P. Evaluation of selected equations for predicting scour at downstream of ski-jump spillway using laboratory and field data. *Eng. Geol.* **2012**, *129*, 98–103. [[CrossRef](#)]
46. Peterka, A.J. *Hydraulic Design of Stilling Basins and Energy Dissipators*; No. 25; US Department of the Interior, Bureau of Reclamation: Washington, DC, USA, 1964.

47. Gunko, F.G.; Burkov, A.F.; Isachenko, N.B.; Rubinstein, G.L.; Soloviova, G.L.; Yuditsky, G.A. Research on the Hydraulic Regime and Local Scour of River Bed below Spillways of High Head Dams. In Proceedings of the 11th IAHR Conference, Leningrad, Russia, 6–11 September 1965.
48. Rajan, B.H.; Rao, K.N. Design of trajectory buckets. *Water Energy Int.* **1980**, *37*, 63–76.
49. Pellegrino, R.; Toledo, M.Á.; Aragoncillo, V. Discharge Flow Rate for the Initiation of Jet Flow in Sky-Jump Spillways. *Water* **2020**, *12*, 1814. [[CrossRef](#)]
50. Breusers HN, C.; Nicollet, G.; Shen, H.W. Local scour around cylindrical piers. *J. Hydraul. Res.* **1977**, *15*, 211–252. [[CrossRef](#)]
51. Whittaker, J. *Scour Related to Energy Dissipators for Head Structure*; N.73 Mitteilungs der Versuchsanstalt für Wasserbau, Hydrologie und Glaziologie, Zurich; 1984. Available online: <https://ethz.ch/content/dam/ethz/special-interest/baug/vaw/vaw-dam/documents/das-institut/mitteilungen/1980-1989/073.pdf> (accessed on 12 June 2023).
52. Hakanson, L. *A Manual of Lake Morphometry*; Springer: New York, NY, USA, 1981.

Disclaimer/Publisher’s Note: The statements, opinions and data contained in all publications are solely those of the individual author(s) and contributor(s) and not of MDPI and/or the editor(s). MDPI and/or the editor(s) disclaim responsibility for any injury to people or property resulting from any ideas, methods, instructions or products referred to in the content.